



# Calculations of the structural and optoelectronic properties of cubic $\text{Cd}_x\text{Zn}_{1-x}\text{Se}_y\text{Te}_{1-y}$ semiconductor quaternary alloys using the DFT-based FP-LAPW approach

Syantika Chanda<sup>1</sup> · Debankita Ghosh<sup>1</sup> · Bimal Debnath<sup>1</sup> · Manish Debbarma<sup>1</sup> · Rahul Bhattacharjee<sup>1,2</sup> · Surya Chattopadhyaya<sup>1</sup>

Published online: 31 October 2019  
© Springer Science+Business Media, LLC, part of Springer Nature 2019

## Abstract

The structural and optoelectronic properties of technologically important  $\text{Cd}_x\text{Zn}_{1-x}\text{Se}_y\text{Te}_{1-y}$  quaternary alloys have been calculated using the density functional theory (DFT)-based full potential (FP)-linearized augmented plane wave (LAPW) approach. The exchange–correlation potentials are calculated using the Perdew–Burke–Ernzerhof (PBE)-generalized gradient approximation (GGA) scheme for the structural properties and both the modified Becke–Johnson (mBJ) and Engel–Vosko (EV)-GGA schemes for the optoelectronic properties. A direct bandgap ( $\Gamma$ – $\Gamma$ ) is observed for all the examined compositions in the  $\text{Cd}_x\text{Zn}_{1-x}\text{Se}_y\text{Te}_{1-y}$  quaternary system. At each cationic (Cd) concentration  $x$ , the lattice constant decreases while the bulk modulus and bandgap increase nonlinearly with increasing anionic (Se) concentration  $y$ . On the other hand, a nonlinear increase in the lattice constant but a decrease in the bulk modulus and bandgap are observed with increasing cationic concentration  $x$  at each anionic concentration  $y$ . The contour maps calculated for the lattice constant and energy bandgap will be useful for designing new quaternary alloys with desired optoelectronic properties. Several interesting features are observed based on the study of the optical properties of the alloys. The compositional dependence of each calculated zero-frequency limit shows the opposite trend, while each calculated critical point shows a similar trend, with respect to that found for the compositional dependence of the bandgap. Finally, the results of these calculations suggest that ZnTe, InAs, GaSb, and InP are suitable substrates for the growth of several zincblende  $\text{Cd}_x\text{Zn}_{1-x}\text{Se}_y\text{Te}_{1-y}$  quaternary alloys.

**Keywords** CdZnSeTe quaternary alloys · mBJ and EV-GGA · Structural properties · Optoelectronic properties · Lattice matching · ZnTe, InAs, GaSb, and InP substrates

## 1 Introduction

In materials science and engineering, alloy formation is used to control various physical properties of semiconductors, especially the magnitude of the bandgap and hence the optoelectronic properties, to achieve the requirements for certain

applications of semiconductor devices. Although this may be achievable through the formation of ternary alloys, the possibility of the formation of quaternary alloys opens a further avenue and represents an enhanced technique to tune various physical properties of semiconductors more precisely and hence widen their applications.

Group IIB–VIA semiconductors such as ZnSe, ZnTe, CdSe, and CdTe are well-known materials for use in microelectronic and optoelectronic applications. The ambient phases of both ZnSe and ZnTe [1] as well as CdSe and CdTe [2] include cubic zincblende (B3) and wurtzite (B4). CdSe and CdTe are widely used as efficient optical materials in the manufacture of visual displays, solid-state laser devices, photodetectors and sensors, light-emitting diodes, blue–green laser diodes [3–5], photovoltaic devices and solar cells [6–9], high-quality quantum rods and their heterostructures [10], nanocrystals [11–13], nanowires [14,

**Electronic supplementary material** The online version of this article (<https://doi.org/10.1007/s10825-019-01409-0>) contains supplementary material, which is available to authorized users.

✉ Surya Chattopadhyaya  
surya\_ju@yahoo.com

<sup>1</sup> Department of Physics, Tripura University, Suryamaninagar, Agartala, Tripura 799022, India

<sup>2</sup> Department of Physics, Women's College, Agartala, Tripura 799001, India

15], quantum dots [16, 17], CdTe nanorod arrays for efficient solar energy conversion [18], etc. On the other hand, both ZnSe and ZnTe are widely used in the manufacture of blue–green laser diodes [19], optical waveguides [20], and wide-bandgap heterostructure lasers [21].

The potential of such materials for use in different application areas has been established based on experimental studies of the electronic structure [22–25], optical properties [26, 27], and elastic properties [28, 29] of bulk CdSe, CdTe, ZnSe, and ZnTe. Experimentally, growth and optical characterization of CdSe thin films [30], characterization of the photosensitivity of CdSe thin films [31], photovoltaic applications of CdTe thin films [32], optical characterization of nanocrystalline CdTe thin films for solar cell applications [33], optical characterization of ZnSe thin films [34], deposition as well as structural and electrical characterization of ZnTe thin films [35], photoluminescence study of ZnTe thin films [36], structural and optical characterization of ZnTe epilayers [37], etc. have been performed for use in different potential applications.

In the case of bulk group II–VI ternary alloys, as well as their thin films and nanostructures, experiments have identified  $n$ -CdSe<sub>0.7</sub>Te<sub>0.3</sub>/ $p$ -CdSe<sub>0.15</sub>Te<sub>0.85</sub> alloys as efficient materials for use in solar cells [38], CdSe<sub>*x*</sub>Te<sub>1–*x*</sub> nanocrystal solar cells as a highly efficient and cost-effective alternative to conventional silicon-based photovoltaic cells [39], and CdSe<sub>*x*</sub>Te<sub>1–*x*</sub> alloy nanocrystals as an efficient materials for use in graded-bandgap solar cells [40]. In addition, the synthesis of rod-shaped/irregular dot-shaped CdSe<sub>*x*</sub>Te<sub>1–*x*</sub> semiconductor nanocrystals for the fabrication of solar cells [41], the synthesis of colloidal ZnTe<sub>1–*x*</sub>Se<sub>*x*</sub> quantum dot (QD) semiconductor alloys as well as the study of the composition and size dependence of their optical gaps [42], the solution-phase synthesis of ZnSe<sub>*x*</sub>Te<sub>1–*x*</sub> ternary alloy nanowires as well as the study of their bandgap bowing [43], the synthesis, optical characterization, and application-oriented studies of ZnSe<sub>*x*</sub>Te<sub>1–*x*</sub> ternary alloy nanowires [44], etc. have been performed. Growth and characterization of zincblende Zn<sub>*x*</sub>Cd<sub>1–*x*</sub>Se single-crystal films [30], ZnCdSe heterostructures [45], ZnCdSe/ZnSe quantum well (QW) structures [46], and ZnCdSe–ZnSSe multiple quantum well (MQW) structures [47] have been performed due to their versatile optoelectronic and photovoltaic applications. Also, the growth and characterization of CdZnTe thin films have been performed for their photovoltaic applications [48] as well as for photoinduced electrical data storage [49]. Moreover, close-spaced vacuum sublimation deposition of thick polycrystalline Cd<sub>1–*x*</sub>Zn<sub>*x*</sub>Te films and their structural and optical characterization were performed by Znamenshchikov and coworkers [50]. Wang and coworkers prepared promising materials to design more cost-effective solar cells by manipulating the depletion region of Cd<sub>*x*</sub>Zn<sub>1–*x*</sub>Te nanocrystal solar cells [51]. Levy and coworkers showed that compositional

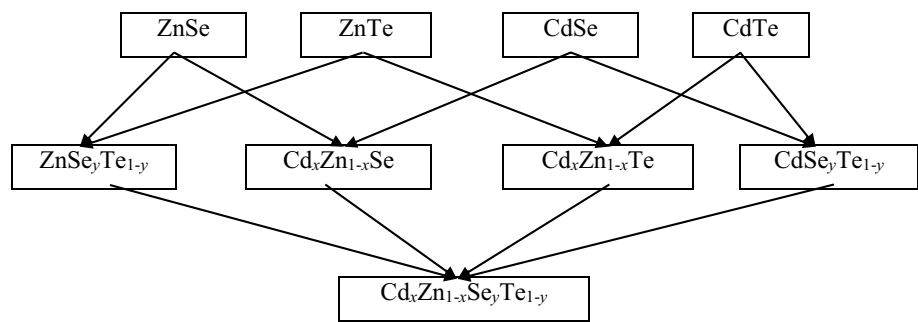
tuning of the optical bandgap, electronic states, and electrochemical potential of ternary Zn<sub>1–*x*</sub>Cd<sub>*x*</sub>Te quantum dots (QDs) can endow them with the ability to address the growing threat of antimicrobial-resistant infections [52].

In the case of cadmium–zinc chalcogenide quaternary alloys, several experimental studies have been performed to date. Molecular beam epitaxial (MBE) growth of Cd<sub>1–*y*</sub>Zn<sub>*y*</sub>Se<sub>*x*</sub>Te<sub>1–*x*</sub> quaternary alloys was performed by Chen and coworkers [53]. Moreover, ZnCdSeTe layers are efficient active layers for light-emitting diodes (LEDs) and laser diodes (LDs) emitting in the red to yellow–green range [54]. MBE-grown Zn<sub>1–*y*</sub>Cd<sub>*y*</sub>Se<sub>*x*</sub>Te<sub>1–*x*</sub> layers on GaAs substrates are suitable for the formation of ZnSe/ZnCdSeTe heterostructures [55]. Spray pyrolysis growth of CdZnSeTe and their optical and electrical characterization were performed by Gaikwad and coworkers [56]. Cd<sub>0.9</sub>Zn<sub>0.1</sub>Te<sub>0.98</sub>Se<sub>0.02</sub> with compositional homogeneity and reduced defects was grown by Roy and coworkers as a new gamma-ray spectroscopic material, having a wide range of applications in medical imaging, nonproliferation, high-energy physics, and astrophysics [57].

On the theoretical side, the structural, elastic, electronic, optical, and thermodynamic properties, etc., of bulk diatomic zincblende CdSe and CdTe [58–72], ZnSe and ZnTe [68–84], bulk pure CdSe<sub>1–*x*</sub>Te<sub>*x*</sub> ternary alloys [85–87], and ZnSe<sub>*x*</sub>Te<sub>1–*x*</sub> [88–92] as well as bulk mixed ternary alloys Cd<sub>*x*</sub>Zn<sub>1–*x*</sub>Se [93, 94] and Cd<sub>1–*x*</sub>Zn<sub>*x*</sub>Te [95–98] have been studied in the framework of different DFT-based approaches, especially the FP-LAPW approach, and applying a variety of different exchange–correlation potential schemes. Theoretical studies on some other chalcogenide ternary alloys with zinc or cadmium as one of the constituents have also been performed [99, 100]. Moreover, based on first-principles calculations, Zhou proposed various possible structures for two-dimensional (2D) ZnX and CdX ( $X = S, Se, \text{ and } Te$ ) materials, which have applications in energy storage and conversion due to their unique electronic structure and optical properties [101].

In the case of bulk quaternary CdZnSeTe alloys, theoretical studies have been carried out on topics such as the optical properties of zincblende Cd<sub>*x*</sub>Zn<sub>1–*x*</sub>Se<sub>*y*</sub>Te<sub>1–*y*</sub> under the conditions of lattice matching to a ZnTe substrate using the pseudopotential approach in the virtual crystal approximation (VCA) [102] and the electronic band structure of Zn<sub>*y*</sub>Cd<sub>1–*y*</sub>Se<sub>*x*</sub>Te<sub>1–*x*</sub> quaternary alloy involving the effects of compositional disorder and bond relaxation using a tight-binding formalism within the VCA [103]. However, those studies covered a very limited number of compounds and properties. Therefore, a detailed theoretical study of various properties of all the compounds in the Cd<sub>*x*</sub>Zn<sub>1–*x*</sub>Se<sub>*y*</sub>Te<sub>1–*y*</sub> quaternary system using an appropriate exchange–correlation (XC) potential scheme is necessary across the whole range of Cd concentration ( $x$ ) and Se concentration ( $y$ ).

**Fig. 1** A schematic diagram showing the formation of the ternary and quaternary alloys in the  $\text{Cd}_x\text{Zn}_{1-x}\text{Se}_y\text{Te}_{1-y}$  system from their basic constituent binary compounds



The results of the first-principles calculations of the structural, electronic, and optical properties of cubic  $\text{Cd}_x\text{Zn}_{1-x}\text{Se}_y\text{Te}_{1-y}$  quaternary alloys as well as the corresponding binary and ternary compositions are reported herein across the whole range of cationic ( $x$ ) and anionic ( $y$ ) concentrations ( $x, y = 0.0, 0.25, 0.50, 0.75, \text{ and } 1.0$ ) using reliable XC potential schemes. Moreover, the dependence of the said properties on the anionic (Se) concentration ( $y$ ) and cationic (Cd) concentration ( $x$ ) is investigated in detail. The results of these calculations suggest new experiments and that such alloys could be potential candidates for use in different optoelectronic and photovoltaic applications.

## 2 Computational details

Density functional theory (DFT) [104, 105] has proven to be one of the most accurate methods for the computation of the electronic structure of solids [106–112]. The DFT-based full-potential linearized augmented plane wave (FP-LAPW) methodology [113] has been implemented successfully in the WIEN2k code [114, 115], and is used to calculate the structural, electronic, and optical properties of binary, ternary, and quaternary materials in the  $\text{Cd}_x\text{Zn}_{1-x}\text{Se}_y\text{Te}_{1-y}$  quaternary system in the present study. For the structural properties, the XC potentials are calculated using the Perdew–Burke–Ernzerhof generalized gradient approximation (PBE-GGA) scheme [116], while the modified Becke–Johnson (mBJ) [117, 118] and Engel–Vosko generalized gradient approximation (EV-GGA) [119] schemes are utilized for efficient calculations of the XC potentials for the electronic and optical properties. For visualization purposes and to carry out some analyses, the graphical code XCrySDen [120] is also applied in the present study.

In the FP-LAPW approach, Kohn–Sham wavefunctions inside non-overlapping muffin-tin spheres surrounding the atomic sites are expanded in spherical harmonics with a maximum value of the angular momentum of  $l_{\text{max}} = 10$ . The same are expanded using a plane-wave basis set in the interstitial region of the unit cell using a cut-off value of  $K_{\text{max}} = 8.0/R_{\text{MT}}$ , where  $R_{\text{MT}}$  is the smallest muffin-tin radius and  $K_{\text{max}}$  is the magnitude of the largest  $K$ -vector in the

plane wave expansion. The potential and charge density Fourier expansion parameter  $G_{\text{max}}$  is taken as  $16 \text{ Ry}^{1/2}$ . The  $R_{\text{MT}}$  values of Cd, Zn, Se, and Te are taken as 2.4, 2.5, 2.3, and 2.5 a.u., respectively. The Brillouin zone integrations are performed using a mesh of 5000  $k$ -points. Both the plane wave cut-off and the number of  $k$ -points are varied to ensure total energy convergence, achieved via self-consistent field (SCF) calculations, when the energy is less than a threshold value of  $10^{-5} \text{ Ry}$ .

The  $\text{Cd}_x\text{Zn}_{1-x}\text{Se}_y\text{Te}_{1-y}$  quaternary system is surrounded by two cationic ternary systems, viz.  $\text{Cd}_x\text{Zn}_{1-x}\text{Se}$  and  $\text{Cd}_x\text{Zn}_{1-x}\text{Te}$ , as well as two anionic ternary systems, viz.  $\text{ZnSe}_y\text{Te}_{1-y}$  and  $\text{CdSe}_y\text{Te}_{1-y}$ . They are again formed from the four binary compounds ZnSe, ZnTe, CdSe, and CdTe. Therefore, the eight-atom  $1 \times 1 \times 1$  cubic zincblende unit cell of these binary compounds is designed by using the experimental lattice parameters of ZnSe, ZnTe, CdSe, and CdTe [26] in the introductory stage. The eight-atom cubic anionic ternary (pseudobinary) alloys  $\text{ZnSe}_y\text{Te}_{1-y}$  and  $\text{CdSe}_y\text{Te}_{1-y}$  with  $y = 0.25, 0.50, \text{ and } 0.75$  are designed by successive substitution of Te atom(s) with Se atom(s) in the  $1 \times 1 \times 1$  unit cell of ZnTe and CdTe, respectively. Similarly, the eight-atom cubic cationic ternary alloys  $\text{Cd}_x\text{Zn}_{1-x}\text{Se}$  and  $\text{Cd}_x\text{Zn}_{1-x}\text{Te}$  with  $x = 0.25, 0.50, \text{ and } 0.75$  are designed by successive replacement of Zn atom(s) with Cd atom(s) in the  $1 \times 1 \times 1$  unit cell of ZnSe and ZnTe, respectively. The quaternary (pseudoternary) alloys  $\text{Cd}_x\text{Zn}_{1-x}\text{Se}_y\text{Te}_{1-y}$  with  $x = 0.25, 0.50, \text{ and } 0.75$  are designed by using a cationic substitution process, i.e., consecutive substitution of Zn atom(s) with Cd atom(s) in the cubic unit cells of the anionic ternary alloys  $\text{ZnSe}_y\text{Te}_{1-y}$  ( $y = 0.25, 0.50, \text{ and } 0.75$ ), and each of the resultant nine quaternary structures is also an eight-atom cubic cell. They can also be formed from the other three ternary systems by cationic/anionic substitution. A schematic diagram of the procedure for the formation of the ternary and quaternary alloys from their basic constituent binaries [121] is shown in Fig. 1. The crystal structures of the nine newly designed quaternary materials in the  $\text{Cd}_{0.25}\text{Zn}_{0.75}\text{Se}_y\text{Te}_{1-y}$ ,  $\text{Cd}_{0.50}\text{Zn}_{0.50}\text{Se}_y\text{Te}_{1-y}$ , and  $\text{Cd}_{0.75}\text{Zn}_{0.25}\text{Se}_y\text{Te}_{1-y}$  systems are shown in Supplementary Figs. S1(a–c), S2(a–c), and S3(a–c), respectively, for  $y = 0.25, 0.50, \text{ and } 0.75$  in the Electronic Supplementary Material.

**Table 1** A matrix presenting the qualitative nature of each specimen with different  $x$  and  $y$  values

$x$	$y$				
	0.0	0.25	0.50	0.75	1.0
0.0	B	T	T	T	B
0.25	T	Q	Q	Q	T
0.50	T	Q	Q	Q	T
0.75	T	Q	Q	Q	T
1.0	B	T	T	T	B

$B$  binary,  $T$  ternary,  $Q$  quaternary

In the present study, the concentration dependence of the structural, electronic, and optical properties of the  $\text{Cd}_x\text{Zn}_{1-x}\text{Se}_y\text{Te}_{1-y}$  quaternary system is investigated in two ways. In the first way, we consider the entire anionic concentration range with  $y=0.0, 0.25, 0.50, 0.75,$  and  $1.0$  at each of five cationic concentrations, viz.  $x=0.0, 0.25, 0.50, 0.75,$  and  $1.0$ , and hence investigate the effects of successive anionic substitution on these properties at each of the cationic concentrations. In the second way, we consider the entire cationic concentration range with  $x=0.0, 0.25, 0.50, 0.75,$  and  $1.0$  at each of five anionic concentrations  $y=0.0, 0.25, 0.50, 0.75,$  and  $1.0$  and investigate the effects of successive cationic substitution on the aforesaid properties at each of the anionic concentrations. In both ways, the qualitative nature of the specimens in each subsystem, formed at either fixed  $x$  or  $y$ , is similar, as shown in matrix form in Table 1.

## 3 Results and discussion

### 3.1 Structural properties

The structural properties of the binary, ternary, and quaternary specimens in the  $\text{Cd}_x\text{Zn}_{1-x}\text{Se}_y\text{Te}_{1-y}$  quaternary system are computed using the structural optimization technique, where the total energy of each of the designed unit cells is minimized with respect to the cell parameters as well as the atomic positions. The total energy of each unit cell at different volumes around the equilibrium unit cell volume are calculated using the self-consistent field (SCF) technique, and the resultant parabolic variation is fit using Murnaghan's equation of state [122], yielding the ground-state structural parameters, such as the minimum energy ( $E_0$ ), equilibrium volume ( $V_0$ ), equilibrium lattice parameter ( $a_0$ ), bulk modulus ( $B_0$ ), and first-order pressure derivative of the bulk modulus ( $B'_0$ ), for each sample (Table 2). Some available experimental and earlier theoretical structural data for the specimens are also included in Table 2 for comparison.

### 3.1.1 The lattice constant and bulk modulus of the binary, ternary, and quaternary specimens

For the binary compounds ZnSe and ZnTe, our computed structural data can be compared with some available experimental  $a_0, B_0,$  and  $B'_0$  data [22, 23, 28]. In the case of the other pair of binary compounds, i.e., CdSe and CdTe, only experimental  $a_0$  and  $B_0$  data [22, 23] are available, while no  $B'_0$  data are available for comparison. Our computed  $a_0$  and  $B_0$  values for ZnSe, ZnTe, CdSe, and CdTe are in excellent agreement with the respective experimental data. In the case of  $B'_0$  of this pair of zinc chalcogenides, our computed data for ZnSe is overestimated by 0.271 while that for ZnTe is underestimated by 0.278, with respect to the corresponding experimental data [22, 28]. Our computed  $a_0, B_0,$  and  $B'_0$  data for the said binary compounds can also be compared with some available earlier theoretical data for ZnSe and ZnTe [70, 71, 73, 77, 79–84, 91] as well as CdSe and CdTe [60, 61, 63–66, 68, 70, 71, 86, 87], revealing good agreement between our computed lattice constant and bulk modulus data for the binaries and several corresponding sets of earlier theoretical data.

No experimental structural data for the anionic ternary alloys  $\text{ZnSe}_y\text{Te}_{1-y}$  and  $\text{CdSe}_y\text{Te}_{1-y}$  or cationic ternary alloys  $\text{Cd}_x\text{Zn}_{1-x}\text{Se}$  and  $\text{Cd}_x\text{Zn}_{1-x}\text{Te}$  are unavailable for comparison. However, our computed  $a_0$  and  $B_0$  data for these ternary alloys can be compared with a few available earlier theoretical data for the corresponding specimens in the  $\text{ZnSe}_y\text{Te}_{1-y}$  [91],  $\text{CdSe}_y\text{Te}_{1-y}$  [86, 87], and  $\text{Cd}_x\text{Zn}_{1-x}\text{Se}$  [94] systems as well as earlier theoretical  $a_0$  data for ternary alloys in the  $\text{Cd}_x\text{Zn}_{1-x}\text{Te}$  system [96]. The calculated  $a_0$  value for each of the anionic ternary alloys  $\text{ZnSe}_y\text{Te}_{1-y}$  and  $\text{CdSe}_y\text{Te}_{1-y}$  as well as the cationic ternary alloys  $\text{Cd}_x\text{Zn}_{1-x}\text{Se}$  is marginally underestimated, while the  $B_0$  value calculated for each of them is marginally overestimated with respect to the corresponding earlier theoretical data. On the other hand, we note marginal overestimation of our calculated  $a_0$  value compared with the corresponding earlier theoretical data in case of each of the ternary alloys in the  $\text{Cd}_x\text{Zn}_{1-x}\text{Te}$  system.

In the case of the quaternary specimens in the  $\text{Cd}_x\text{Zn}_{1-x}\text{Se}_y\text{Te}_{1-y}$  system, we are unable to compare our computed structural data due to the lack of such experimental or earlier theoretical data in the literature.

### 3.1.2 The concentration dependence of the lattice constant and bulk modulus

In the present study, the concentration dependence of  $a_0$  and  $B_0$  for the specimens in the  $\text{Cd}_x\text{Zn}_{1-x}\text{Se}_y\text{Te}_{1-y}$  quaternary system is investigated over the entire cationic and anionic concentration range with  $x/y=0.0, 0.25, 0.50, 0.75,$  and  $1.0$ . At each of the five specified cationic (Cd) concentrations  $x$ , it is observed that the lattice constant  $a_0$  decreases nonlinearly

**Table 2** The calculated  $a_0$ ,  $B_0$ , and  $B'$  values of the specimens in the  $Cd_xZn_{1-x}Se_yTe_{1-y}$  quaternary system

$x$	$y$	Specimen	$a_0$ (Å)	$B_0$ (GPa)	$B'$
0.0	0.0	ZnTe	6.109	48.39	4.762
			6.104, <sup>a</sup> 6.089 <sup>b</sup>	50.9 <sup>a</sup>	5.04 <sup>a</sup>
			6.020, <sup>a1</sup> 6.150, <sup>b1</sup> 6.103, <sup>c1</sup> 6.063, <sup>d1</sup> 6.00, <sup>e1</sup>	49.2, <sup>a1</sup> 52.9, <sup>c1</sup> 50.54, <sup>d1</sup> 5.21, <sup>e1</sup> 51.23, <sup>f1</sup>	4.60 <sup>e1</sup>
			6.078, <sup>f1</sup> 6.195 <sup>a2</sup>	43.60, <sup>a2</sup>	
	0.25	ZnSe <sub>0.25</sub> Te <sub>0.75</sub>	6.085	49.86	4.776
			6.099 <sup>a2</sup>	45.63 <sup>a2</sup>	
	0.50	ZnSe <sub>0.50</sub> Te <sub>0.50</sub>	5.977	53.03	5.108
			5.989 <sup>a2</sup>	48.90 <sup>a2</sup>	
	0.75	ZnSe <sub>0.75</sub> Te <sub>0.25</sub>	5.859	56.73	5.632
			5.873 <sup>a2</sup>	52.14 <sup>a2</sup>	
1.0	ZnSe	5.688	63.37	4.499	
		5.67, <sup>a</sup> 5.669, <sup>b</sup> 5.667, <sup>c</sup>	62.50, <sup>a</sup> 64.7, <sup>c</sup>	4.77 <sup>c</sup>	
		5.591, <sup>a1</sup> 5.638, <sup>c1</sup> 5.666, <sup>d1</sup> 5.624, <sup>e1</sup> 5.630, <sup>f1</sup>	83.3, <sup>a1</sup> 65.2, <sup>c1</sup> 62.32, <sup>d1</sup> 71.82, <sup>e1</sup> 63.34, <sup>f1</sup>	4.88, <sup>e1</sup> 4.67, <sup>h1</sup> 4.02, <sup>i1</sup> 4.599 <sup>j1</sup>	
		5.409, <sup>g1</sup> 5.618, <sup>h1</sup> 5.544, <sup>i1</sup> 5.741, <sup>j1</sup> 5.747, <sup>a2</sup>	67.6, <sup>h1</sup> 72.44, <sup>i1</sup> 71.84, <sup>j1</sup> 56.77 <sup>a2</sup>		
0.25	0.0	Cd <sub>0.25</sub> Zn <sub>0.75</sub> Te	6.191	45.72	4.431
			6.18 <sup>a3</sup>		
	0.25	Cd <sub>0.25</sub> Zn <sub>0.75</sub> Se <sub>0.25</sub> Te <sub>0.75</sub>	6.173	48.14	4.398
	0.50	Cd <sub>0.25</sub> Zn <sub>0.75</sub> Se <sub>0.50</sub> Te <sub>0.50</sub>	6.112	49.61	4.621
	0.75	Cd <sub>0.25</sub> Zn <sub>0.75</sub> Se <sub>0.75</sub> Te <sub>0.25</sub>	5.996	52.89	4.942
	1.0	Cd <sub>0.25</sub> Zn <sub>0.75</sub> Se	5.878	57.93	4.206
		5.933 <sup>b3</sup>	49.40 <sup>b3</sup>	3.335 <sup>b3</sup>	
0.50	0.0	Cd <sub>0.50</sub> Zn <sub>0.50</sub> Te	6.326	43.59	4.346
			6.31 <sup>a3</sup>		
	0.25	Cd <sub>0.50</sub> Zn <sub>0.50</sub> Se <sub>0.25</sub> Te <sub>0.75</sub>	6.281	44.72	4.406
	0.50	Cd <sub>0.50</sub> Zn <sub>0.50</sub> Se <sub>0.50</sub> Te <sub>0.50</sub>	6.228	47.03	4.383
	0.75	Cd <sub>0.50</sub> Zn <sub>0.50</sub> Se <sub>0.75</sub> Te <sub>0.25</sub>	6.115	50.05	4.625
	1.0	Cd <sub>0.50</sub> Zn <sub>0.50</sub> Se	5.998	54.42	4.235
		6.058 <sup>b3</sup>	46.46 <sup>b3</sup>	3.126 <sup>b3</sup>	
0.75	0.0	Cd <sub>0.75</sub> Zn <sub>0.25</sub> Te	6.391	42.96	4.195
			6.38 <sup>a3</sup>		
	0.25	Cd <sub>0.75</sub> Zn <sub>0.25</sub> Se <sub>0.25</sub> Te <sub>0.75</sub>	6.363	43.05	4.299
	0.50	Cd <sub>0.75</sub> Zn <sub>0.25</sub> Se <sub>0.50</sub> Te <sub>0.50</sub>	6.321	45.31	4.344
	0.75	Cd <sub>0.75</sub> Zn <sub>0.25</sub> Se <sub>0.75</sub> Te <sub>0.25</sub>	6.218	47.79	4.563
	1.0	Cd <sub>0.75</sub> Zn <sub>0.25</sub> Se	6.095	50.82	4.076
		6.172 <sup>b3</sup>	43.67 <sup>b3</sup>	3.63 <sup>b3</sup>	
1.0	0.0	CdTe	6.478	41.01	4.525
			6.48 <sup>a,b</sup>	44.5 <sup>a</sup>	
			6.447, <sup>a1</sup> 6.568, <sup>b1</sup> 6.48, <sup>k1</sup> 6.631, <sup>l1</sup> 6.44, <sup>m1</sup>	34.3, <sup>a1</sup> 48.94, <sup>k1</sup> 33.79, <sup>l1</sup> 46.6, <sup>m1</sup> 46.8, <sup>n1</sup>	4.47, <sup>k1</sup> 5.14, <sup>l1</sup> 5.3 <sup>n1</sup>
			6.64, <sup>n1</sup> 6.46, <sup>o1</sup> 6.43, <sup>p1</sup> 5.884, <sup>q1</sup> 6.620, <sup>b2</sup>	38.08, <sup>o1</sup> 46.0, <sup>p1</sup> 66.6, <sup>q1</sup> 36.242, <sup>b2</sup> 33.793 <sup>c2</sup>	
			6.631 <sup>c2</sup>		
	0.25	CdSe <sub>0.25</sub> Te <sub>0.75</sub>	6.463	41.38	4.712
			6.526, <sup>b2</sup> 6.532 <sup>c2</sup>	40.138, <sup>b2</sup> 38.864 <sup>c2</sup>	
	0.50	CdSe <sub>0.50</sub> Te <sub>0.50</sub>	6.418	43.44	5.007
			6.407 <sup>b2</sup> , 6.438 <sup>c2</sup>	42.206 <sup>b2</sup> , 40.864 <sup>c2</sup>	
	0.75	CdSe <sub>0.75</sub> Te <sub>0.25</sub>	6.306	45.88	5.394
		6.322, <sup>b2</sup> 6.331 <sup>c2</sup>	43.079, <sup>b2</sup> 43.549 <sup>c2</sup>		
1.0	CdSe	6.118	50.38	4.413	
		6.05, <sup>a</sup> 6.084 <sup>b</sup>	53.0 <sup>a</sup>		
		6.035, <sup>a1</sup> 6.052, <sup>b1</sup> 6.05, <sup>k1</sup> 6.216, <sup>l1</sup> 6.0412, <sup>m1</sup>	66.5, <sup>a1</sup> 65.12, <sup>k1</sup> 45.16, <sup>l1</sup> 59.2, <sup>m1</sup> 52.4, <sup>n1</sup>	4.20, <sup>k1</sup> 4.58, <sup>l1</sup> 5.1, <sup>n1</sup> 4.13 <sup>r1</sup>	
		6.16, <sup>n1</sup> 6.04, <sup>o1</sup> 6.207, <sup>b2</sup> 6.216 <sup>c2</sup>	51.02, <sup>o1</sup> 61.0, <sup>r1</sup> 45.60, <sup>b2</sup> 44.86 <sup>c2</sup>		

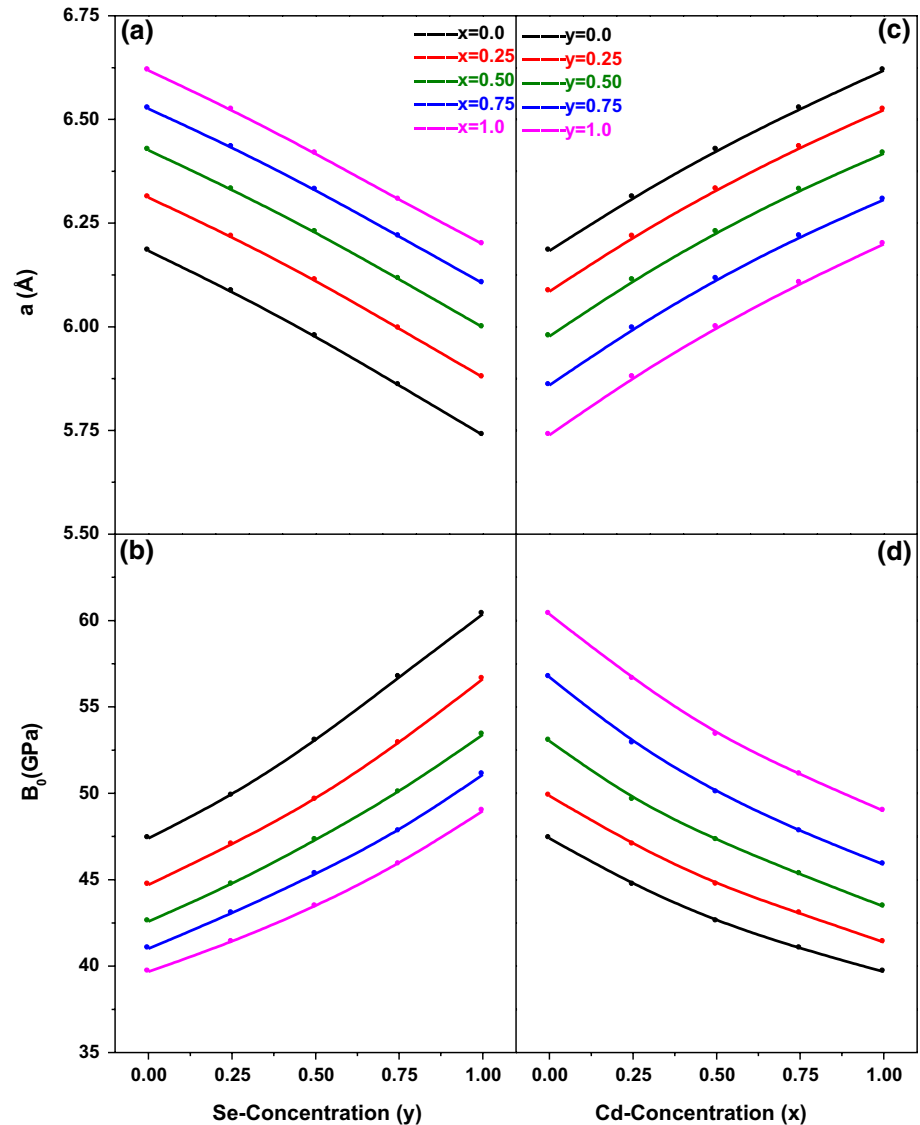
Experimental data: <sup>a</sup>Ref. [22], <sup>b</sup>Ref. [23], <sup>c</sup>Ref. [28]

Earlier theoretical data: <sup>a1</sup>Ref. [70], <sup>b1</sup>Ref. [71], <sup>c1</sup>Ref. [77], <sup>d1</sup>Ref. [80], <sup>e1</sup>Ref. [83], <sup>f1</sup>Ref. [84], <sup>g1</sup>Ref. [73], <sup>h1</sup>Ref. [79], <sup>i1</sup>Ref. [81], <sup>j1</sup>Ref. [82], <sup>k1</sup>Ref. [60], <sup>l1</sup>Ref. [61], <sup>m1</sup>Ref. [63], <sup>n1</sup>Ref. [64], <sup>o1</sup>Ref. [65], <sup>p1</sup>Ref. [66], <sup>q1</sup>Ref. [68], <sup>r1</sup>Ref. [62]

Earlier theoretical data: <sup>a2</sup>Ref. [91], <sup>b2</sup>Ref. [86], <sup>c2</sup>Ref. [87]

Earlier theoretical data: <sup>a3</sup>Ref. [96], <sup>b3</sup>Ref. [94]

**Fig. 2** The variation of the calculated **a**  $a_0$  with the Se concentration  $y$  at each of the fixed Cd concentrations  $x$ , **b**  $B_0$  with the Se concentration  $y$  at each of the fixed Cd concentrations  $x$ , **c**  $a_0$  with the Cd concentration  $x$  at each of the fixed Se concentrations  $y$ , and **d**  $B_0$  with the Cd concentration  $x$  at each of the fixed Se concentrations  $y$  for the specimens in the  $\text{Cd}_x\text{Zn}_{1-x}\text{Se}_y\text{Te}_{1-y}$  quaternary system



with increasing anionic (Se) concentration  $y$ , and each such variation is shown in Fig. 2a. In this case, the substitution of tellurium atom(s) of greater radius (1.23 Å) with selenium atom(s) of smaller radius (1.03 Å) decreases the volume of the cubic unit cell and thereby the lattice constant  $a_0$ . Due to the inverse proportionality between the lattice constant and bulk modulus, a nonlinear increase in  $B_0$  and hence the hardness of the specimen with increasing anionic (Se) concentration  $y$  at each of the five aforesaid cationic concentrations  $x$  is shown in Fig. 2b.

Again, at each of the five fixed values of the anionic (Se) concentration  $y$ , the lattice constant  $a_0$  is observed to increase nonlinearly with increasing cationic (Cd) concentration  $x$ , with each such variation being shown in Fig. 2c. The substitution of zinc atom(s) of smaller radius (1.42 Å) with cadmium atom(s) of greater radius (1.61 Å) is responsible for the increase in the cubic unit cell volume and thereby

the lattice constant  $a_0$ . From this, we observe a nonlinear decrease in the bulk modulus  $B_0$  and hence the hardness of the specimen with increasing cationic (Cd) concentration  $x$  at each of the five aforesaid anionic concentrations  $y$ , as shown in Fig. 2d.

For an ideal alloy system, Vegard's law [123] suggests a linear concentration ( $x/y$ ) dependence (LCD) for the lattice constant ( $a_0$ ), while experimental studies [124, 125] confirm a nonlinear variation in a real alloy system, having the form

$$a(x) = \alpha_a + \beta_a x + \delta_a x^2. \quad (1)$$

The nonlinear coefficient  $\delta_a$  is known as the bowing parameter of the lattice constant versus concentration curve for any real alloy system, and can be calculated by fitting the corresponding  $a_0$  versus concentration ( $x/y$ ) curve using Eq. 1. A similar quadratic relationship can also quantitatively explain the nonlinearity in the concentration dependence of

**Table 3** The bowing parameters calculated from the concentration dependence curves of  $a_0$  and  $B_0$

Alloy system	Fixed concentration	Variable concentration	$\delta_a$ (Å)	$\delta_B$ (GPa)
ZnSe <sub>y</sub> Te <sub>1-y</sub>	x	y	-0.0651	3.006
Cd <sub>0.25</sub> Zn <sub>0.75</sub> Se <sub>y</sub> Te <sub>1-y</sub>	x	y	-0.0617	3.108
Cd <sub>0.50</sub> Zn <sub>0.50</sub> Se <sub>y</sub> Te <sub>1-y</sub>	x	y	-0.0594	3.280
Cd <sub>0.75</sub> Zn <sub>0.25</sub> Se <sub>y</sub> Te <sub>1-y</sub>	x	y	-0.0560	3.634
CdSe <sub>y</sub> Te <sub>1-y</sub>	x	y	-0.0484	3.977
Cd <sub>x</sub> Zn <sub>1-x</sub> Te	y	x	-0.0986	5.074
Cd <sub>x</sub> Zn <sub>1-x</sub> Se <sub>0.25</sub> Te <sub>0.75</sub>	y	x	-0.1097	4.834
Cd <sub>x</sub> Zn <sub>1-x</sub> Se <sub>0.50</sub> Te <sub>0.50</sub>	y	x	-0.1134	3.954
Cd <sub>x</sub> Zn <sub>1-x</sub> Se <sub>0.75</sub> Te <sub>0.25</sub>	y	x	-0.1202	3.714
Cd <sub>x</sub> Zn <sub>1-x</sub> Se	y	x	-0.1303	3.383

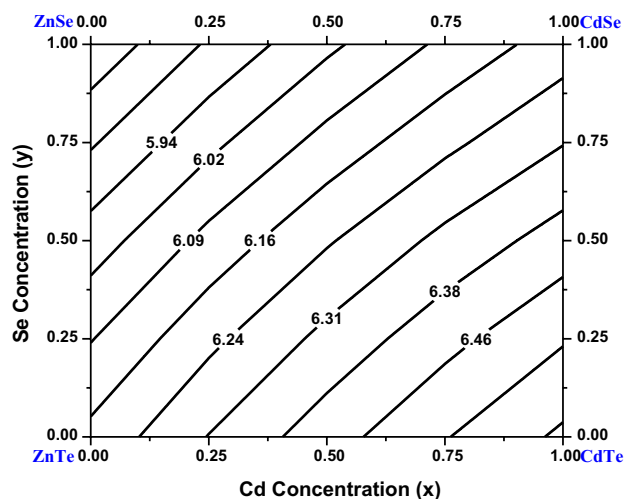
the bulk modulus in any real alloy system, where the nonlinear coefficient  $\delta_B$  measures the bowing in the bulk modulus versus concentration curve.

Here, the  $a_0$  versus  $y$  curve at each of the cationic concentrations  $x$  as well as  $a_0$  versus  $x$  curve at each of the anionic concentrations  $y$  shows marginal upward bowing due to the marginal mismatch between the lattice constants of the terminal binary/ternary compounds. On the other hand, each of the  $B_0$  versus  $y$  as well as  $B_0$  versus  $x$  curves at each fixed  $x$  and  $y$ , respectively, exhibits small downward bowing due to the small mismatch between the bulk modulus of the corresponding terminal binary/ternary compounds. In the case of the lattice constant as well as the bulk modulus versus anionic/cationic concentration curves, the respective calculated bowing parameters  $\delta_a$  and  $\delta_B$  are presented in Table 3. It is observed that  $\delta_a$  decreases while  $\delta_B$  increases gradually as one proceeds from ZnSe<sub>y</sub>Te<sub>1-y</sub> to CdSe<sub>y</sub>Te<sub>1-y</sub> via consecutive replacement of Zn with Cd atom(s). In contrast,  $\delta_a$  increases while  $\delta_B$  decreases gradually as one proceeds from Cd<sub>x</sub>Zn<sub>1-x</sub>Te to Cd<sub>x</sub>Zn<sub>1-x</sub>Se via consecutive replacement of Te with Se atom(s).

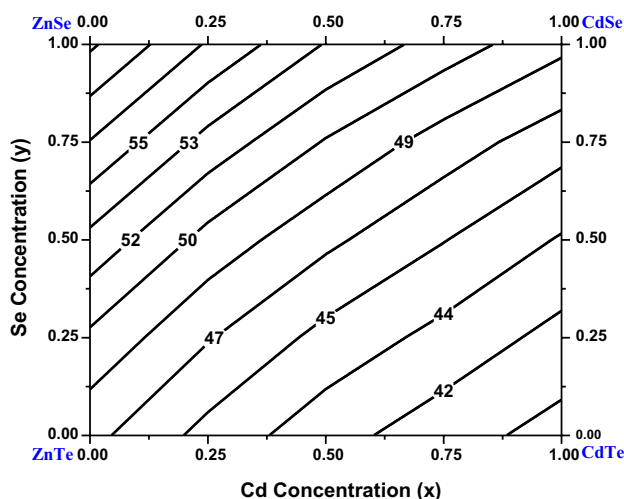
The calculated contour plots for  $a_0$  versus  $x$  and  $y$  are shown in Fig. 3a, while that for  $B_0$  versus  $x$  and  $y$  is shown in Fig. 3b in the case of the Cd<sub>x</sub>Zn<sub>1-x</sub>Se<sub>y</sub>Te<sub>1-y</sub> quaternary system, where deviations of both  $a_0$  and  $B_0$  in each system from their respective LCD can be observed again. The  $a_0$  or  $B_0$  of any ternary or quaternary specimen corresponding to any  $x/y$  composition in the range  $0 \leq x, y \leq 1$  can be evaluated from the corresponding contour plot.

### 3.2 Electronic properties

The experimental or theoretical study of the electronic properties of any semiconductor is necessary to investigate its appropriateness for the fabrication of microelectronic or optoelectronic devices. In the present work, density



(a)



(b)

**Fig. 3** The contour maps of the calculated **a** lattice constant  $a_0$  and **b** bulk modulus  $B_0$  versus the compositions  $x$  and  $y$  for the Cd<sub>x</sub>Zn<sub>1-x</sub>Se<sub>y</sub>Te<sub>1-y</sub> quaternary alloys

functional calculations of the electronic properties of the binary, ternary, and quaternary specimens in the Cd<sub>x</sub>Zn<sub>1-x</sub>Se<sub>y</sub>Te<sub>1-y</sub> quaternary system are performed using the mBJ and EV-GGA schemes for the computation of the necessary XC potentials. The bandgap for each of the said specimens calculated using both XC functionals is presented in Table 4. In addition, some available experimental as well as some earlier theoretical bandgap values are also presented in Table 4 for comparison. Table 4 also shows that, in the case of each of the specimens under consideration and for both XC functionals employed, the calculated bandgap follows the trend  $E_g^{mBJ} > E_g^{EV-GGA}$ .

**Table 4** The minimum bandgap ( $E_g$ ) of the specimens in the  $\text{Cd}_x\text{Zn}_{1-x}\text{Se}_y\text{Te}_{1-y}$  quaternary system calculated using the mBJ and EV-GGA functionals

x	y	Specimen	Energy bandgap (eV)	
			EV-GGA	mBJ
0.0	0.0	ZnTe	1.899	2.405
			2.39 <sup>a,b</sup>	
	0.25	$\text{ZnSe}_{0.25}\text{Te}_{0.75}$	1.33, <sup>a1</sup> 2.27, <sup>b1</sup> 1.32, <sup>c1</sup> 1.95, <sup>d1</sup> 1.28, <sup>e1</sup> 2.4, <sup>f1</sup> 1.021, <sup>a2S</sup> 1.577 <sup>a2*</sup>	2.426
			1.925	
			0.862, <sup>a2S</sup> 1.457 <sup>a2*</sup>	
0.50	$\text{ZnSe}_{0.50}\text{Te}_{0.50}$	1.975	2.502	
		0.835, <sup>a2S</sup> 1.448 <sup>a2*</sup>		
0.75	$\text{ZnSe}_{0.75}\text{Te}_{0.25}$	2.068	2.636	
		0.906, <sup>a2S</sup> 1.545 <sup>a2*</sup>		
1.0	ZnSe	2.171	2.869	
		2.82, <sup>a,c</sup> 2.87 <sup>b</sup>		
0.25	0.0	$\text{Cd}_{0.25}\text{Zn}_{0.75}\text{Te}$	1.658	2.347
			1.27 <sup>b3</sup>	
	0.25	$\text{Cd}_{0.25}\text{Zn}_{0.75}\text{Se}_{0.25}\text{Te}_{0.75}$	1.727	2.370
			1.811	
	0.50	$\text{Cd}_{0.25}\text{Zn}_{0.75}\text{Se}_{0.50}\text{Te}_{0.50}$	1.834	2.519
			1.887	
1.0	$\text{Cd}_{0.25}\text{Zn}_{0.75}\text{Se}$	1.887	2.842	
		0.76 <sup>a3S</sup>		
0.50	0.0	$\text{Cd}_{0.50}\text{Zn}_{0.50}\text{Te}$	1.508	2.252
			1.31 <sup>b3</sup>	
	0.25	$\text{Cd}_{0.50}\text{Zn}_{0.50}\text{Se}_{0.25}\text{Te}_{0.75}$	1.539	2.285
			1.598	
	0.50	$\text{Cd}_{0.50}\text{Zn}_{0.50}\text{Se}_{0.50}\text{Te}_{0.50}$	1.624	2.466
1.662				
0.75	0.0	$\text{Cd}_{0.75}\text{Zn}_{0.25}\text{Te}$	1.432	2.039
			1.40 <sup>b3</sup>	
	0.25	$\text{Cd}_{0.75}\text{Zn}_{0.25}\text{Se}_{0.25}\text{Te}_{0.75}$	1.463	2.116
			1.496	
	0.50	$\text{Cd}_{0.75}\text{Zn}_{0.25}\text{Se}_{0.50}\text{Te}_{0.50}$	1.512	2.233
			1.537	
1.0	$\text{Cd}_{0.75}\text{Zn}_{0.25}\text{Se}$	1.537	2.273	
		0.49 <sup>a3S</sup>		
1.0	0.0	CdTe	1.308	1.609
			1.606, <sup>a</sup> 1.60 <sup>b</sup>	
	0.25	$\text{CdSe}_{0.25}\text{Te}_{0.75}$	0.80, <sup>a1</sup> 0.65, <sup>c1</sup> 1.60, <sup>l1</sup> 1.52, <sup>m1</sup> 1.88, <sup>n1</sup> 0.588, <sup>o1</sup> 1.98, <sup>p1</sup> 0.546, <sup>q1</sup> 1.91, <sup>r1</sup> 0.76, <sup>b2S</sup> 1.31, <sup>b2*</sup> 0.588, <sup>c2S</sup> 1.087 <sup>c2*</sup>	1.775
			1.365	
			0.79, <sup>b2S</sup> 1.44, <sup>b2*</sup> 0.549, <sup>c2S</sup> 1.13 <sup>c2*</sup>	
	0.50	$\text{CdSe}_{0.50}\text{Te}_{0.50}$	1.397	1.817
			0.83, <sup>b2S</sup> 1.56, <sup>b2*</sup> 0.512, <sup>c2S</sup> 1.17 <sup>c2*</sup>	
0.75	$\text{CdSe}_{0.75}\text{Te}_{0.25}$	1.432	1.884	
		0.89, <sup>b2S</sup> 1.65, <sup>b2*</sup> 0.492, <sup>c2S</sup> 1.18 <sup>c2*</sup>		
1.0	CdSe	1.464	1.901	
		1.90, <sup>a</sup> 1.82 <sup>b</sup>		
		0.76, <sup>a1</sup> 0.45, <sup>c1</sup> 1.39, <sup>m1</sup> 1.08, <sup>n1</sup> 0.475, <sup>o1</sup> 1.20, <sup>p1</sup> 0.575, <sup>q1</sup> 2.49, <sup>r1</sup> 0.95, <sup>b2S</sup> 1.76, <sup>b2*</sup> 0.475, <sup>c2S</sup> 1.2 <sup>c2*</sup>		

Experimental data: <sup>a</sup>Ref. [22], <sup>b</sup>Ref. [24], <sup>c</sup>Ref. [25]

Earlier theoretical data: <sup>a1</sup>Ref. [69], <sup>b1</sup>Ref. [75], <sup>c1</sup>Ref. [70], <sup>d1</sup>Ref. [77], <sup>e1</sup>Ref. [73], <sup>h1</sup>Ref. [74], <sup>i1</sup>Ref. [76], <sup>j1</sup>Ref. [78], <sup>k1</sup>Ref. [82], <sup>l1</sup>Ref. [58], <sup>m1</sup>Ref. [71], <sup>n1</sup>Ref. [60], <sup>o1</sup>Ref. [61], <sup>e1</sup>Ref. [83], <sup>f1</sup>Ref. [84], <sup>p1</sup>Ref. [62], <sup>q1</sup>Ref. [64], <sup>r1</sup>Ref. [65]

Earlier theoretical data: <sup>a2\*</sup>Ref. [90] ⇒ EV-GGA, <sup>a2S</sup>Ref. [90] ⇒ PBE-GGA, <sup>b2\*</sup>Ref. [86] ⇒ EV-GGA, <sup>b2S</sup>Ref. [86] ⇒ PBE-GGA, <sup>c2\*</sup>Ref. [87] ⇒ EV-GGA, <sup>c2S</sup>Ref. [87] ⇒ PBE-GGA

Earlier theoretical data: <sup>a3S</sup>Ref. [94] ⇒ PBE-GGA, <sup>b3</sup>Ref. [96] ⇒ LDA



### 3.2.1 Band structure

The band structure computed for each of the binary compounds ZnSe, ZnTe, CdSe, and CdTe exhibits a direct minimum bandgap ( $\Gamma$ - $\Gamma$ ) in the zincblende phase when using both XC functionals. Some experimental observations for ZnSe and ZnTe [22, 24, 25] as well as CdS and CdSe [22, 24] also support such qualitative features of the respective calculated band structures. The ternary specimens in the  $\text{ZnSe}_y\text{Te}_{1-y}$ ,  $\text{CdSe}_y\text{Te}_{1-y}$ ,  $\text{Cd}_x\text{Zn}_{1-x}\text{Te}$ , and  $\text{Cd}_x\text{Zn}_{1-x}\text{Se}$  systems also indicate a direct bandgap ( $\Gamma$ - $\Gamma$ ). Although no experimental information is available regarding the qualitative features of the band structure of any of these ternary alloys, the computed results can be compared with some respective earlier theoretical findings for  $\text{ZnSe}_y\text{Te}_{1-y}$  [90],  $\text{CdSe}_y\text{Te}_{1-y}$  [86, 87],  $\text{Cd}_x\text{Zn}_{1-x}\text{Se}$  [94], and  $\text{Cd}_x\text{Zn}_{1-x}\text{Te}$  [96], revealing good agreement. In the case of the band structure of each of the nine quaternary specimens in the  $\text{Cd}_x\text{Zn}_{1-x}\text{Se}_y\text{Te}_{1-y}$  system, a direct fundamental bandgap ( $\Gamma$ - $\Gamma$ ) is also observed. However, we cannot find any experimental observations or earlier theoretical studies on the band structure of these quaternary specimens to compare them. Such newly designed direct-bandgap, optically active quaternary semiconductor materials may be useful for the manufacture of faster and highly efficient optoelectronic devices [126]. The band structure of the nine quaternary specimens in the  $\text{Cd}_{0.25}\text{Zn}_{0.75}\text{Se}_y\text{Te}_{1-y}$ ,  $\text{Cd}_{0.50}\text{Zn}_{0.50}\text{Se}_y\text{Te}_{1-y}$ , and  $\text{Cd}_{0.75}\text{Zn}_{0.25}\text{Se}_y\text{Te}_{1-y}$  systems are presented in Figs. S4(a–c), S5(a–c), and S6(a–c), respectively, for  $y = 0.25, 0.50,$  and  $0.75$ , in the Electronic Supplementary Materials.

### 3.2.2 The bandgap of the binary, ternary, and quaternary specimens

From Table 4, it is observed that the experimental fundamental bandgap ( $E_g$ ) for the binary compounds ZnSe and ZnTe [22, 24, 25] as well as CdSe and CdTe [22, 24] is in excellent agreement with our corresponding data calculated using the mBJ functional, while the results calculated using the EV-GGA functional are much smaller than the corresponding experimental outcomes. Only one set of earlier theoretical bandgap data for ZnSe and ZnTe [84] agree well with our corresponding data calculated using the mBJ functional, although they are 0.069 eV and 0.005 eV smaller compared with our mBJ-based data. In the case of the Cd chalcogenides, a set of earlier theoretical bandgap data for CdSe [84] and CdTe [58] agree excellently with our corresponding mBJ-based data, although they are 0.141 eV and 0.009 eV smaller compared with our respective mBJ-based results.

No experimental bandgap data for any of the anionic or cationic ternary alloys are available in the literature for comparison. In the case of all the anionic ternary specimens in

the  $\text{ZnSe}_y\text{Te}_{1-y}$  and  $\text{CdSe}_y\text{Te}_{1-y}$  systems as well as the cationic ternary specimens in the  $\text{Cd}_x\text{Zn}_{1-x}\text{Se}$  and  $\text{Cd}_x\text{Zn}_{1-x}\text{Te}$  systems, both our mBJ- and EV-GGA-based calculated bandgap values for each ternary specimen are well overestimated with respect to corresponding earlier theoretical data for  $\text{ZnSe}_y\text{Te}_{1-y}$  [90] and  $\text{CdSe}_y\text{Te}_{1-y}$  [86, 87] alloys calculated using the PBE-GGA and EV-GGA functional as well as for  $\text{Cd}_x\text{Zn}_{1-x}\text{Se}$  [94] alloys using the PBE-GGA functional and for  $\text{Cd}_x\text{Zn}_{1-x}\text{Te}$  [96] alloys using the local density approximation (LDA) functional. Again, no experimental or earlier theoretical bandgap data for any of the nine quaternary specimens in the  $\text{Cd}_x\text{Zn}_{1-x}\text{Se}_y\text{Te}_{1-y}$  system are available in literature for comparison.

### 3.2.3 The concentration dependence of the bandgap

An investigation of the cationic ( $x$ ) and anionic ( $y$ ) concentration ( $x/y = 0.0, 0.25, 0.50, 0.75,$  and  $1.0$ ) dependence of the fundamental energy bandgap ( $E_g$ ) of the specimens in the  $\text{Cd}_x\text{Zn}_{1-x}\text{Se}_y\text{Te}_{1-y}$  quaternary system is presented in this subsection. At each of the five fixed cationic (Cd) concentrations  $x$ , the calculated  $E_g$  is observed to increase nonlinearly with increasing anionic (Se) concentration ( $y$ ), with each such variation being shown in Fig. 4a and b for the mBJ and EV-GGA functional, respectively. On the other hand, at each of the five fixed anionic (Se) concentrations  $y$ , the calculated  $E_g$  is observed to decrease nonlinearly with increasing cationic (Cd) concentration ( $x$ ), with each such variation calculated using the mBJ and EV-GGA functional being shown in Fig. 4c and d, respectively.

For any real alloy system, the nonlinear concentration dependence of the bandgap ( $E_g$ ) can be expressed as

$$E_g(x) = \alpha_g + \beta_g x + \delta_g x^2, \quad (2)$$

where  $E_g(x)$  is the concentration-dependent bandgap and the nonlinear coefficient  $\delta_g$  is called the bandgap bowing or optical bowing parameter. For any specific XC functional, the bandgap bowing coefficient  $\delta_g$  for each alloy system can be calculated by fitting the  $E_g$  versus  $x$  or  $y$  curve using Eq. 2.

Here, the  $E_g$  versus  $y$  curves at each Cd concentration ( $x$ ) as well as the  $E_g$  versus  $x$  curves at each Se concentration ( $y$ ) show downward bowing when employing both XC functionals. The  $\delta_g$  value calculated from each  $E_g$  versus anionic/cationic concentration curve when using both XC functionals is presented in Table 5. It is clear from Table 5 that  $\delta_g$  gradually decreases when employing both XC functionals as one proceeds from  $\text{ZnSe}_y\text{Te}_{1-y}$  to  $\text{CdSe}_y\text{Te}_{1-y}$  with consecutive replacement of Zn with Cd atom(s). On the other hand,  $\delta_g$  gradually increases when using both XC functionals as one proceeds from  $\text{Cd}_x\text{Zn}_{1-x}\text{Te}$  to  $\text{Cd}_x\text{Zn}_{1-x}\text{Se}$  with successive replacement of Te with Se atom(s). No experimental or

**Fig. 4** The variation of the **a** mBJ-calculated minimum bandgap  $E_g$  with the Se concentration  $y$  at each of the fixed Cd concentrations  $x$ , **b** EV-GGA-calculated minimum bandgap  $E_g$  with the Se concentration  $y$  at each of the fixed Cd concentrations  $x$ , **c** mBJ-calculated minimum bandgap  $E_g$  with the Cd concentration  $x$  at each of the fixed Se concentrations  $y$ , and **d** EV-GGA-calculated minimum bandgap  $E_g$  with the Cd concentration  $x$  at each of the fixed Se concentrations  $y$  of the specimens in the  $\text{Cd}_x\text{Zn}_{1-x}\text{Se}_y\text{Te}_{1-y}$  quaternary system

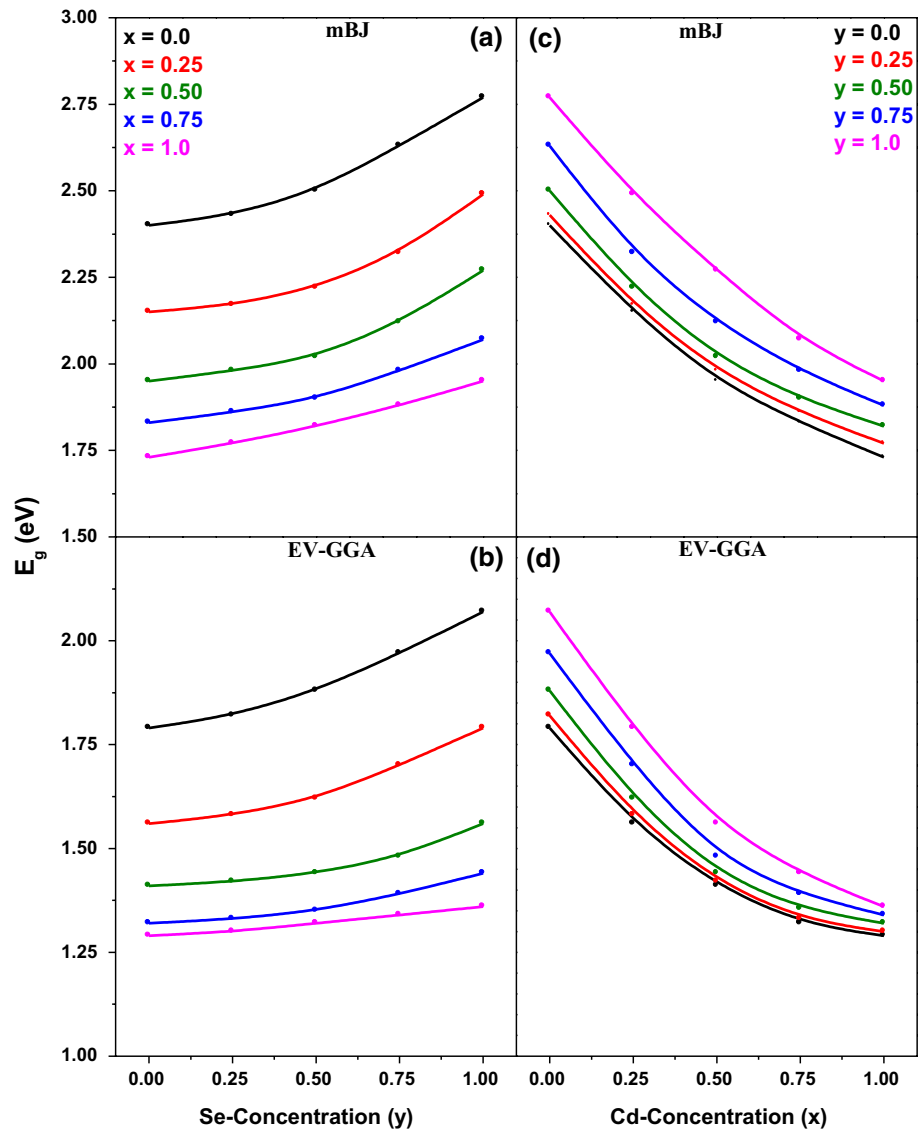


**Table 5** The optical bowing parameters ( $\delta_g$ ) calculated from the concentration dependence curves of  $E_g$

Alloy system	Fixed concentration	Variable concentration	$\delta_g$ (eV)	
			mBJ	EV-GGA
$\text{ZnSe}_y\text{Te}_{1-y}$	$x$	$y$	0.406	0.289
$\text{Cd}_{0.25}\text{Zn}_{0.75}\text{Se}_y\text{Te}_{1-y}$	$x$	$y$	0.343	0.224
$\text{Cd}_{0.50}\text{Zn}_{0.50}\text{Se}_y\text{Te}_{1-y}$	$x$	$y$	0.282	0.163
$\text{Cd}_{0.75}\text{Zn}_{0.25}\text{Se}_y\text{Te}_{1-y}$	$x$	$y$	0.183	0.114
$\text{CdSe}_y\text{Te}_{1-y}$	$x$	$y$	0.080	0.023
$\text{Cd}_x\text{Zn}_{1-x}\text{Te}$	$y$	$x$	0.388	0.226
$\text{Cd}_x\text{Zn}_{1-x}\text{Se}_{0.25}\text{Te}_{0.75}$	$y$	$x$	0.434	0.360
$\text{Cd}_x\text{Zn}_{1-x}\text{Se}_{0.50}\text{Te}_{0.50}$	$y$	$x$	0.508	0.423
$\text{Cd}_x\text{Zn}_{1-x}\text{Se}_{0.75}\text{Te}_{0.25}$	$y$	$x$	0.563	0.501
$\text{Cd}_x\text{Zn}_{1-x}\text{Se}$	$y$	$x$	0.624	0.583

earlier theoretical  $\delta_g$  data for any of these systems are available for comparison.

For the  $\text{Cd}_x\text{Zn}_{1-x}\text{Se}_y\text{Te}_{1-y}$  quaternary system, the contour map calculated for  $E_g$  versus the compositions  $x/y$  using the mBJ and EV-GGA functionals is shown in Fig. 5a and b, respectively. From such contour plots, the  $E_g$  value of any ternary or quaternary specimen corresponding to any  $x/y$  compositions in the range  $0 \leq x, y \leq 1$  can be evaluated.

### 3.2.4 The density of states (DOS)

Using the density of states (DOS) of any semiconductor specimen, one can identify the atomic and orbital signature of the various electronic states present in its band structure. In the present study, although we compute the total density of states (TDOS) and partial density of states (PDOS) for each of the specimens in the  $\text{Cd}_x\text{Zn}_{1-x}\text{Se}_y\text{Te}_{1-y}$  quaternary

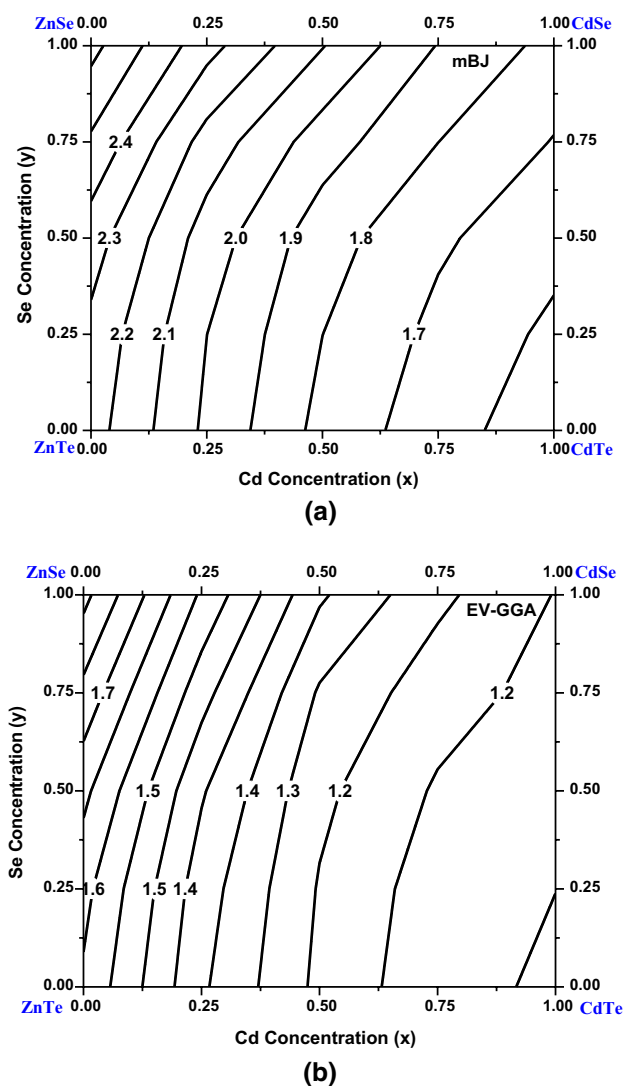


**Fig. 5** The contour maps calculated for the minimum bandgap  $E_g$  versus the compositions  $x$  and  $y$  for the  $\text{Cd}_x\text{Zn}_{1-x}\text{Se}_y\text{Te}_{1-y}$  quaternary alloys using the **a** mBJ or **b** EV-GGA functional

system, only the TDOS (filled gray curves) and PDOS (colored lines) of the ternary and quaternary specimens in the  $\text{Cd}_{0.25}\text{Zn}_{0.75}\text{Se}_y\text{Te}_{1-y}$  system for the whole range of anionic ( $y$ ) concentrations and those in the  $\text{Cd}_x\text{Zn}_{1-x}\text{Se}_{0.25}\text{Te}_{0.75}$  system for the whole range of cationic ( $x$ ) concentrations are presented as representatives in Figs. 6a–e and 7a–e, respectively. In both figures, the contributions of the different atomic orbitals of the constituents of each specimen in both systems in their various regions of valence and conduction bands are clearly presented. Moreover, the effects of gradual anionic ( $y$ ) substitution at fixed cationic ( $x$ ) concentration on the DOS (Fig. 6a–e) as well as the effects of successive cationic ( $x$ ) substitution at fixed anionic ( $y$ ) concentration on the DOS (Fig. 7a–e) are clearly observed.

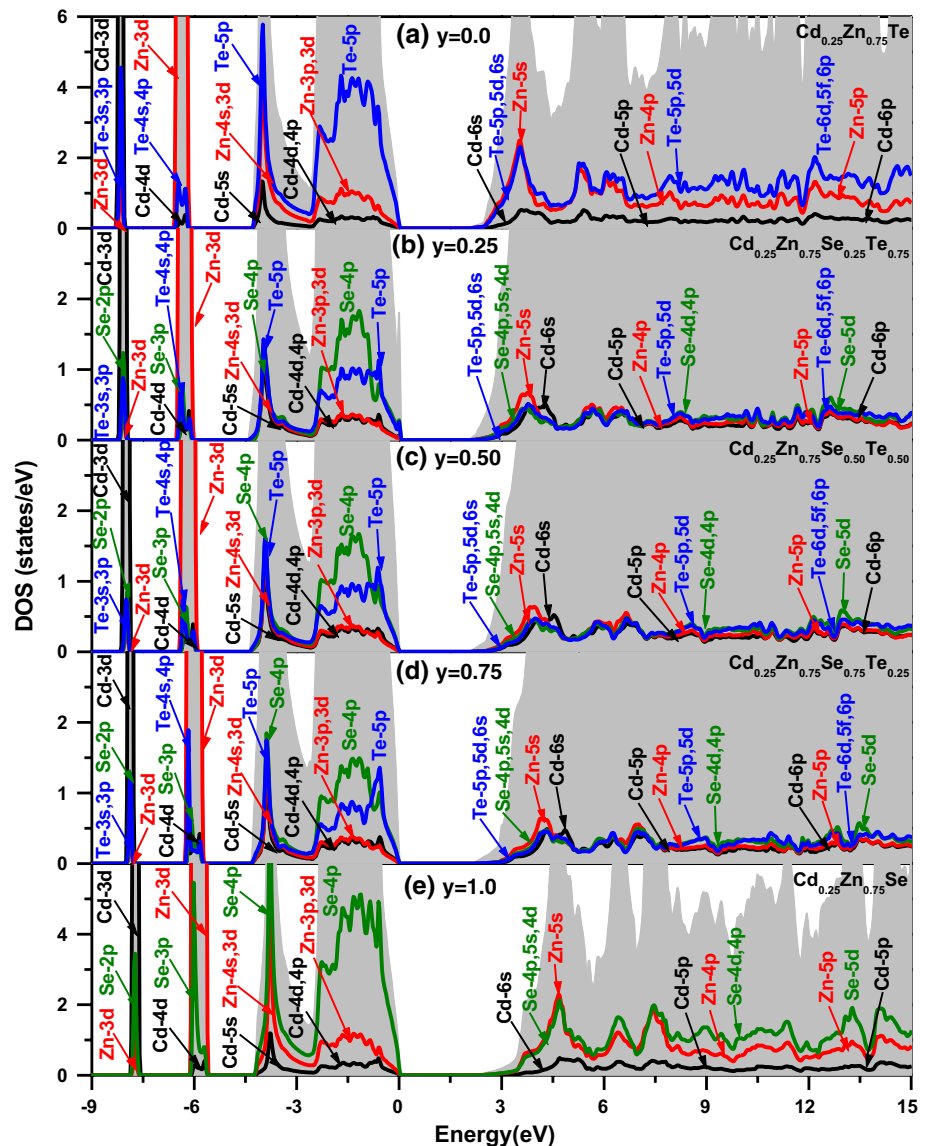
From Figs. 6a and 7a, one can observe from the TDOS and PDOS of the ternary specimens  $\text{Cd}_{0.25}\text{Zn}_{0.75}\text{Te}$  and  $\text{ZnSe}_{0.25}\text{Te}_{0.75}$ , respectively, that the different regions of the valence and conduction bands of the former are dominated by various orbitals of the Cd, Zn, and Te atoms, while the same for the latter are dominated by various orbitals of the Zn, Se, and Te atoms. With increasing doping of Se atom in the former as well as Cd atom in the latter, Figs. 6b–d and 7b–d show that, in different regions of the valence and conduction bands of the successive quaternary specimens, the contribution of the different chalcogen orbitals now results from the combined contribution of selenium and tellurium atoms in the former set, while the contribution of different orbitals of atom(s), other than chalcogens, now comes from combined contributions of Cd and Zn atoms in the latter set. Moreover, in the different valence and conduction band regions of the said specimens, the contribution from different orbitals of Se atom(s) gradually increase while those of Te gradually decrease with increasing Se concentration in the former set, while the contribution from different orbitals of Cd atom(s) gradually increase while those of Zn gradually decrease with increasing Cd concentration in the latter set. Finally, note the complete domination of the different orbitals of Se atoms in the TDOS and PDOS of the ternary specimen  $\text{Cd}_{0.25}\text{Zn}_{0.75}\text{Se}$  in Fig. 6e, and those of Cd atoms in the TDOS and PDOS of the ternary specimen  $\text{CdSe}_{0.25}\text{Te}_{0.75}$  in Fig. 7e. Note that, in the different valence and conduction band regions of the said specimens, the contributions of the atomic orbitals of Cd and Zn in the former set and the contributions of the atomic orbitals of Se and Te in the latter set remain unchanged due to their presence at fixed concentrations in each set.

In both cases, the most interesting part of the DOS for each specimen is the region of the valence and conduction bands closest to the Fermi level, because most of the significant dipole-allowed optical transitions take place between different orbitals in these regions. It is observed from the PDOS of all the specimens in the  $\text{Cd}_{0.25}\text{Zn}_{0.75}\text{Se}_y\text{Te}_{1-y}$  system in Fig. 6a–e or the PDOS of all the specimens in the  $\text{Cd}_x\text{Zn}_{1-x}\text{Se}_{0.25}\text{Te}_{0.75}$  system in Fig. 7a–e that the contributions to the valence band closest to the Fermi level mostly come from chalcogen- $p$  states, i.e., Te- $5p$  or Se- $4p$  or both. On the other hand, the conduction band of these compounds near the Fermi level is dominated almost equally by either Zn- $5s$  or Cd- $6s$  or both of them, as well as collectively by chalcogen- $s$ ,  $p$ , and  $d$  orbitals, i.e., either Te- $5p$ ,  $6s$ ,  $5d$  or Se- $4p$ ,  $5s$ ,  $4d$  or both sets of these chalcogen orbitals.

### 3.3 Optical properties

When an electromagnetic wave is incident on a crystal, electronic excitations take place within it, resulting in the observation of different optical features of the crystal. For any

**Fig. 6** The TDOS (filled gray curves) and PDOS (colored lines) of the specimens in the  $\text{Cd}_{0.25}\text{Zn}_{0.75}\text{Se}_y\text{Te}_{1-y}$  quaternary alloys with **a**  $y=0.0$ , **b**  $y=0.25$ , **c**  $y=0.50$ , **d**  $y=0.75$ , and **e**  $y=1.0$  (Color figure online)



solid, such features are strongly dependent on its electronic properties. The study of the optical properties of a crystal thus provides a clear idea about the nature of its response to incident electromagnetic radiation at a particular frequency, and materials can be selected for the manufacture of optoelectronic devices based on such optical features. The optical features of materials are mainly studied in terms of the frequency-dependent complex dielectric function  $\epsilon(\omega)$ , expressed as [127]:

$$\epsilon(\omega) = \epsilon_1(\omega) + i\epsilon_2(\omega), \quad (3)$$

where the real and imaginary parts of  $\epsilon(\omega)$  are  $\epsilon_1(\omega)$  and  $\epsilon_2(\omega)$ , respectively. The refractive index  $n(\omega)$ , extinction coefficient  $k(\omega)$ , normal incidence reflectivity  $R(\omega)$ , optical conductivity  $\sigma(\omega)$ , optical absorption coefficient  $\alpha(\omega)$ , and energy loss function  $L(\omega)$  of any semiconductor specimen can then be derived from its  $\epsilon_1(\omega)$  and  $\epsilon_2(\omega)$ . Their

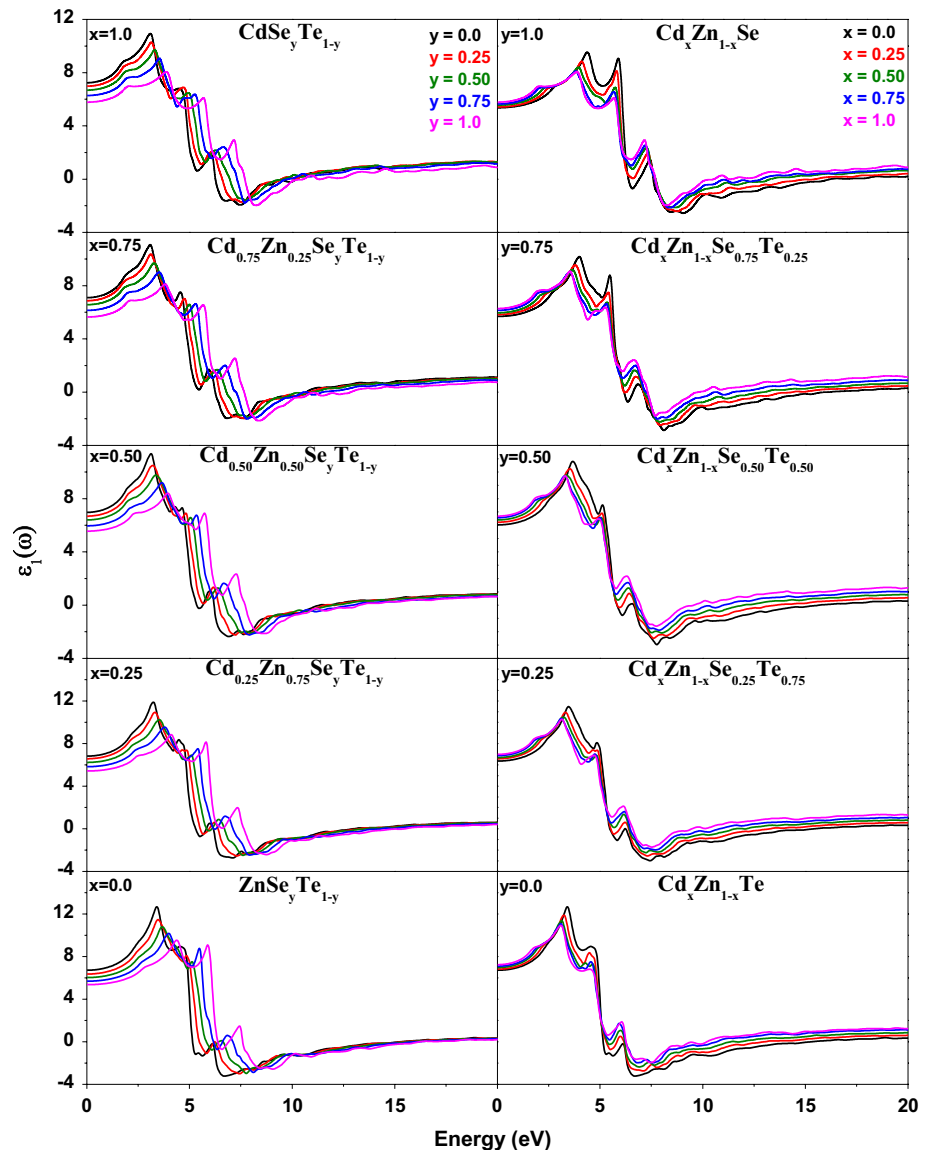
expressions along with some of the ancillary optical parameters are presented as Eqs. SQ1-SQ14 in Sect. I of the Electronic Supplementary Material.

### 3.3.1 The frequency response curves of the different optical parameters

In the present work, we calculate the frequency response of  $\epsilon_1(\omega)$ ,  $\epsilon_2(\omega)$ ,  $n(\omega)$ ,  $k(\omega)$ ,  $R(\omega)$ ,  $\sigma(\omega)$ ,  $\alpha(\omega)$ , and  $L(\omega)$  for the binary, ternary, and quaternary specimens in the  $\text{Cd}_x\text{Zn}_{1-x}\text{Se}_y\text{Te}_{1-y}$  system up to an incident energy of 30.0 eV using Eqs. SQ1-SQ14 and employing both the mBJ and EV-GGA functional. The frequency responses of  $\epsilon_1(\omega)$  and  $\epsilon_2(\omega)$  calculated using the mBJ functional are shown in Figs. 8 and 9, respectively, in the main text, while those of  $n(\omega)$ ,  $k(\omega)$ ,  $R(\omega)$ ,  $\sigma(\omega)$ ,  $\alpha(\omega)$ , and  $L(\omega)$  calculated using the same XC functional are presented in Figs. S7–S12 in the



**Fig. 8** The frequency response curves of  $\epsilon_1(\omega)$  for the specimens in the  $\text{Cd}_x\text{Zn}_{1-x}\text{Se}_y\text{Te}_{1-y}$  quaternary system for the different Se concentrations at each of the Cd concentrations (five left panels) and for the different Cd concentrations at each of the Se concentrations (five right panels)



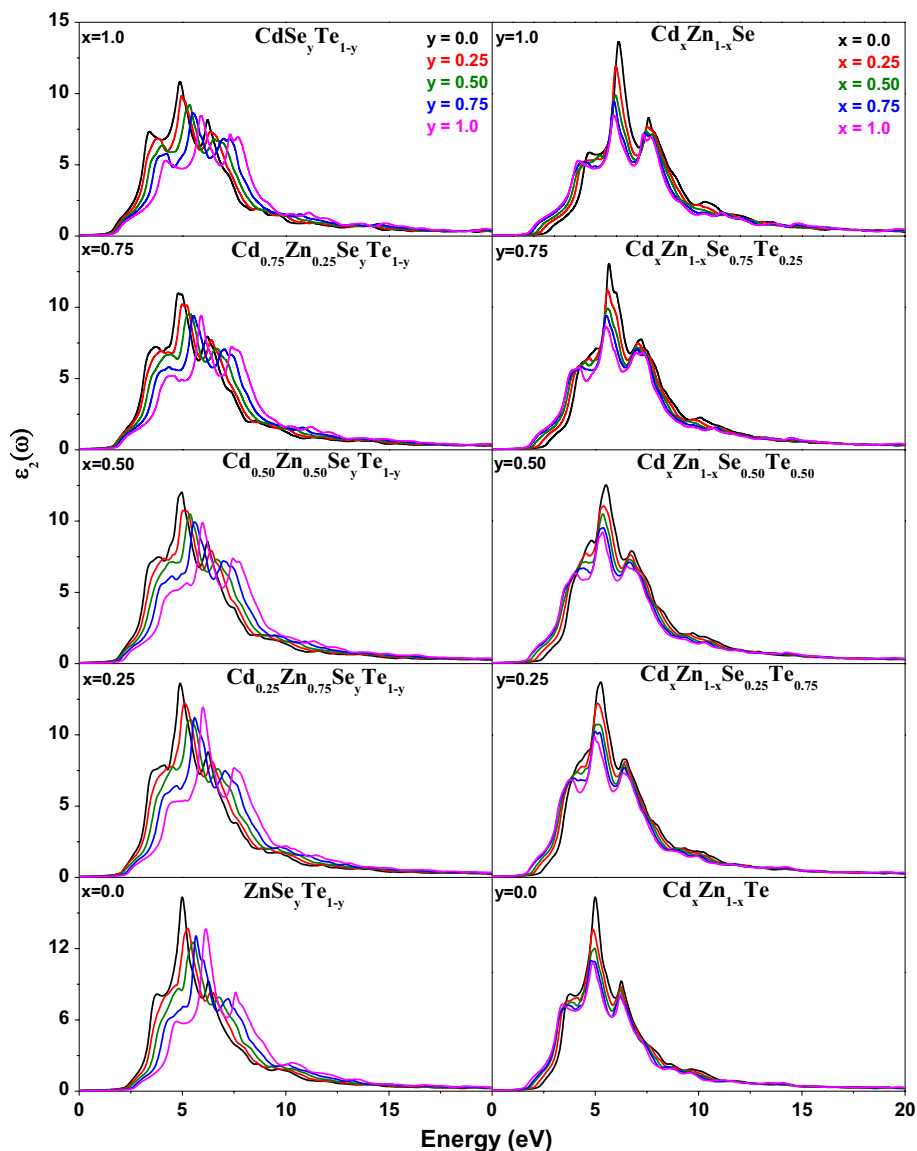
occurrence of the peak(s) in the  $\epsilon_2(\omega)$  spectra of each specimen in the aforesaid energy region.

The most intense peaks in the  $\epsilon_2(\omega)$  spectra of ZnSe and ZnTe at 6.14 eV and 4.99 eV are due to the strong electronic transitions  $\text{Se-}4p \rightarrow \text{Zn-}5s$  and  $\text{Te-}5p \rightarrow \text{Zn-}5s$ , respectively, while the comparatively much lower-intensity peaks at 7.58 eV and 6.24 eV in the  $\epsilon_2(\omega)$  spectra of ZnSe and ZnTe are due to the comparatively much weaker electronic transitions  $\text{Se-}4p \rightarrow \text{Zn-}4p$  and  $\text{Te-}5p \rightarrow \text{Zn-}4p$ , respectively, from the occupied valence to the unoccupied conduction band. On the other hand, the most intense peaks in the  $\epsilon_2(\omega)$  spectra of CdSe and CdTe at 5.89 eV and 4.88 eV are due to the strong electronic transitions  $\text{Se-}4p \rightarrow \text{Cd-}6s$  and  $\text{Te-}5p \rightarrow \text{Cd-}6s$ , respectively, while the weak-intensity peaks at 7.31 eV and 6.22 eV in the  $\epsilon_2(\omega)$  spectra of CdSe and CdTe are due to the comparatively weak electronic transitions  $\text{Se-}4p \rightarrow \text{Cd-}5p$

and  $\text{Te-}5p \rightarrow \text{Cd-}5p$ , respectively, from the occupied valence to the unoccupied conduction band. Note that the intensity difference between the two peaks in the  $\epsilon_2(\omega)$  spectra of each of ZnSe and ZnTe is greater compared with that between the two peaks in the  $\epsilon_2(\omega)$  spectra of each of CdSe and CdTe.

In the case of the  $\epsilon_2(\omega)$  spectra of the anionic ternary specimen  $\text{ZnSe}_{0.25}\text{Te}_{0.75}$ , the first intense peak at 5.26 eV is due to the combined effect of the very strong  $\text{Te-}5p \rightarrow \text{Zn-}5s$  and much weaker  $\text{Se-}4p \rightarrow \text{Zn-}5s$  electronic transitions, while that arising in the  $\epsilon_2(\omega)$  spectra of  $\text{CdSe}_{0.25}\text{Te}_{0.75}$  at 4.97 eV is due to the combined effect of the very strong  $\text{Te-}5p \rightarrow \text{Cd-}6s$  and much weaker  $\text{Se-}4p \rightarrow \text{Cd-}6s$  electronic transitions from the valence to conduction band. On the other hand, the next intense peak at 6.38 eV in the  $\epsilon_2(\omega)$  spectra of  $\text{ZnSe}_{0.25}\text{Te}_{0.75}$  is due to the combined effect of the strong  $\text{Te-}5p \rightarrow \text{Zn-}4p$  and much weaker  $\text{Se-}4p \rightarrow \text{Zn-}4p$  transitions,

**Fig. 9** The frequency response curves of  $\epsilon_2(\omega)$  for the specimens in the  $\text{Cd}_x\text{Zn}_{1-x}\text{Se}_y\text{Te}_{1-y}$  quaternary system for the different Se concentrations at each of the Cd concentrations (five left panels) and for the different Cd concentrations at each of the Se concentrations (five right panels)



while that at 6.39 eV in the  $\epsilon_2(\omega)$  spectra of  $\text{CdSe}_{0.25}\text{Te}_{0.75}$  is due to the combined effect of the strong  $\text{Te-}5p \rightarrow \text{Cd-}5p$  and much weaker  $\text{Se-}4p \rightarrow \text{Cd-}5p$  electronic transitions from the valence to conduction band. It is also observed that the intensity difference between the two peaks in the  $\epsilon_2(\omega)$  spectra of  $\text{ZnSe}_{0.25}\text{Te}_{0.75}$  is greater compared with that between the two peaks in the  $\epsilon_2(\omega)$  spectra of  $\text{CdSe}_{0.25}\text{Te}_{0.75}$ . Note also that the intensity of the transitions originating from  $\text{Se-}4p$  gradually dominates over the transitions originating from  $\text{Te-}5p$  and the peak positions clearly exhibit a marginal blue-shift in both the  $\text{ZnSe}_y\text{Te}_{1-y}$  and  $\text{CdSe}_y\text{Te}_{1-y}$  systems with increasing Se concentration ( $y$ ).

In the case of the  $\epsilon_2(\omega)$  spectra of the cationic ternary specimens  $\text{Cd}_{0.25}\text{Zn}_{0.75}\text{Se}$  and  $\text{Cd}_{0.25}\text{Zn}_{0.75}\text{Te}$ , the first intense peaks at 6.00 eV and 4.88 eV are due to the combined effect of the electronic transitions  $\text{Se-}4p \rightarrow \text{Zn-}5s$ ,  $\text{Se-}4p \rightarrow \text{Cd-}6s$  and  $\text{Te-}5p \rightarrow \text{Zn-}5s$ ,  $\text{Te-}5p \rightarrow \text{Cd-}6s$ , respectively, from

the valence to conduction band. On the other hand, the next intense peaks at 7.52 eV and 6.24 eV are due to the electronic transitions  $\text{Se-}4p \rightarrow \text{Zn-}4p$ ,  $\text{Se-}4p \rightarrow \text{Cd-}5p$  and  $\text{Te-}5p \rightarrow \text{Zn-}4p$ ,  $\text{Te-}5p \rightarrow \text{Cd-}5p$ , respectively, from the valence to conduction band. Also, note the substantial intensity difference between the two peaks in the  $\epsilon_2(\omega)$  spectra of each of the said cationic ternary alloys. Note also that the intensity of the transitions terminating at  $\text{Cd-}6s$ ,  $5p$  gradually dominates over the transitions to  $\text{Zn-}5s$ ,  $4p$  with increasing Cd concentration ( $x$ ) in both the  $\text{Cd}_x\text{Zn}_{1-x}\text{Se}$  and  $\text{Cd}_x\text{Zn}_{1-x}\text{Te}$  systems.

In the case of the  $\epsilon_2(\omega)$  spectra of the nine quaternary specimens  $\text{Cd}_{0.25}\text{Zn}_{0.75}\text{Se}_y\text{Te}_{1-y}$ ,  $\text{Cd}_{0.50}\text{Zn}_{0.50}\text{Se}_y\text{Te}_{1-y}$ , and  $\text{Cd}_{0.75}\text{Zn}_{0.25}\text{Se}_y\text{Te}_{1-y}$  with  $y=0.25, 0.50$ , and  $0.75$ , the first intense peak in each spectra is due to the combined effect of the  $\text{Te-}5p \rightarrow \text{Zn-}5s$ ,  $\text{Te-}5p \rightarrow \text{Cd-}6s$ ,  $\text{Se-}4p \rightarrow \text{Zn-}5s$ , and  $\text{Se-}4p \rightarrow \text{Cd-}6s$  electronic transitions from the valence to

conduction band. On the other hand, the comparatively low-intensity peak in each spectrum at the higher-energy side of the first peak is due to the Te-5p → Zn-4p, Te-5p → Cd-5p, Se-4p → Zn-4p, and Se-4p → Cd-5p electronic transitions from the valence to conduction band. Keeping the Cd concentration ( $x$ ) fixed, if one gradually increases the Se concentration ( $y$ ) to 0.50 then 0.75, the transitions originating from Se-4p become gradually stronger compared with the transitions originating from Te-5p in both peaks in the  $\epsilon_2(\omega)$  spectra of each corresponding quaternary specimen. On the other hand, if one gradually increases the Cd concentration ( $x$ ) to 0.50 then 0.75 while keeping the Se concentration ( $y$ ) fixed, the transitions terminating at Cd-6s, 5p become gradually stronger compared with the transitions terminating at Zn-5s, 4p in both peaks of the  $\epsilon_2(\omega)$  spectra in each corresponding quaternary specimen.

In the frequency response spectra of  $k(\omega)$  of each specimen in Fig. S9,  $k(\omega) > 1$  is observed throughout the incident energy region of 3.5–10.5 eV, with the peaks having a maximum amplitude of  $k(\omega) > 2$ . Therefore, incident photons with energy in this specific range suffer more obstruction during their penetration through each of these specimens compared with photons having energy beyond this energy region in the  $k(\omega)$  spectra [126].

The  $\sigma(\omega)$  spectra of each specimen in Fig. S10 show a couple of peaks in the narrow incident energy region of 4.0–9.0 eV with peak values  $\sigma(\omega)$  greater than at least  $6000 \Omega^{-1} \text{cm}^{-1}$ , while  $\sigma(\omega)$  becomes very low beyond this energy region. The  $\alpha(\omega)$  spectra of each specimen in Fig. S11 show substantial optical absorption [ $\alpha(\omega) > 100$ ] in the 5.0–12.5 eV incident energy region.

The electron energy loss function  $L(\omega)$  is used to investigate electrons inelastically scattered by atoms at lattice site and to calculate the amount of energy loss during such scattering processes. It is obvious from Eq. SQ14 that the  $L(\omega)$  of any specimen will be strongly dependent on its  $\epsilon_2(\omega)$  [128] and that their frequency responses will be qualitatively opposite in nature. In the  $L(\omega)$  spectra of each specimen in Fig. S12, it is observed that  $L(\omega)$  is insignificant because of the significantly high value of  $\epsilon_2(\omega)$  in the energy region up to 10.0 eV. This indicates that inelastic scattering of only a few electrons occurs, resulting in minimum energy loss in this energy region. On the other hand,  $L(\omega)$  gradually increases beyond an incident energy of 10.0 eV because  $\epsilon_2(\omega)$  gradually decreases beyond this energy value. As a result, the number of inelastically scattered electrons and hence the resulting energy loss gradually increase beyond 10.0 eV. It is also observed that  $L(\omega)$  for each specimen is significantly high with multiple peaks in the incident energy region of 11.0–22.0 eV, because  $\epsilon_2(\omega)$  is significantly low (less than unity) in this region. Note that one can measure

the plasma resonance frequency for any specimen from the energetic position of the most intense peak in its  $L(\omega)$  spectra.

### 3.3.2 The zero-frequency limits and critical points in the different optical spectra

The zero-frequency limits  $\epsilon_1(0)$ ,  $n(0)$ , and  $R(0)$  of the  $\epsilon_1(\omega)$ ,  $n(\omega)$ , and  $R(\omega)$  spectra, respectively, are calculated. For any specimen, these give the magnitude of the optical parameters  $\epsilon_1(\omega)$ ,  $n(\omega)$ , and  $R(\omega)$  in the respective spectra at zero incident energy/frequency, which are known as the static dielectric constant, static refractive index, and static reflectivity, respectively. The  $\epsilon_1(0)$ ,  $n(0)$ , and  $R(0)$  values calculated for all of the specimens in the  $\text{Cd}_x\text{Zn}_{1-x}\text{Se}_y\text{Te}_{1-y}$  quaternary system using both the mBJ and EV-GGA functionals are presented in Table 6, along with available experimental or earlier theoretical data for a few specimens for comparison.

Few experimental  $\epsilon_1(0)$  data for ZnSe [26], ZnTe [27], CdSe [26], and CdTe [27] are available for comparison, while no experimental  $\epsilon_1(0)$  data for ternary or quaternary specimens or any experimental  $n(0)$  and  $R(0)$  data for the binary, ternary, and quaternary specimens are available for comparison. Also, some earlier theoretical  $\epsilon_1(0)$  data for ZnSe and ZnTe [68, 72, 97] and CdSe and CdTe [59, 68, 69, 72, 87, 100],  $n(0)$  and  $R(0)$  data for ZnSe and ZnTe [97],  $n(0)$  data for CdSe and CdTe [67, 87, 100], and  $R(0)$  data for CdSe and CdTe are available in literature.

Our mBJ-based computed  $\epsilon_1(0)$  data for the binary compounds ZnSe, ZnTe, CdSe, and CdTe are in excellent agreement with the corresponding experimental data due to the excellent match of our mBJ-based computed bandgaps with the respective experimental findings. On the other hand, our EV-GGA-based  $\epsilon_1(0)$  results for each of ZnSe, ZnTe, CdSe, and CdTe are fairly overestimated with respect to the corresponding experimental data due to the fair underestimation of our EV-GGA-based computed bandgaps with respect to the corresponding experimental data. Each of our mBJ-based calculated  $n(0)$  and  $R(0)$  results for any of the binary specimens is underestimated with respect to the corresponding previously calculated data due to our higher corresponding calculated larger bandgap compared with those reported in earlier theoretical studies.

Only the earlier theoretical  $\epsilon_1(0)$  data for each of the anionic ternary specimens  $\text{CdSe}_y\text{Te}_{1-y}$  calculated using the EV-GGA functional [87] and that for the cationic ternary specimen  $\text{Cd}_{0.25}\text{Zn}_{0.75}\text{Se}$  calculated using the mBJ functional [98] are substantially underestimated with respect to our corresponding data calculated using both the mBJ and EV-GGA functional. In the case of the  $\text{Cd}_{0.25}\text{Zn}_{0.75}\text{Se}$  ternary alloy, our mBJ-based computed  $n(0)$  data are underestimated with



**Table 6** The  $\epsilon_1(0)$ ,  $n(0)$ , and  $R(0)$  values of the binary, ternary, and quaternary specimens in the  $\text{Cd}_x\text{Zn}_{1-x}\text{Se}_y\text{Te}_{1-y}$  system calculated using the mBJ and EV-GGA functionals

x	y	Specimen	Zero-frequency limit										
			$\epsilon_1(0)$		$n(0)$		$R(0)$						
			mBJ	EV-GGA	mBJ	EV-GGA	mBJ	EV-GGA					
0.0	0.0	ZnTe	7.117		7.303		2.592	2.720	0.194	0.213			
			7.28 <sup>a</sup>										
			7.13, <sup>a1</sup> 7.99 <sup>b1</sup>				2.67 <sup>a1</sup>		0.197 <sup>a1</sup>				
			7.7 <sup>c1</sup>										
			6.758		7.125		2.522	2.669	0.177	0.206			
			6.332		6.788		2.456	2.605	0.168	0.198			
			6.090		6.414		2.385	2.532	0.157	0.188			
			5.724		5.953		2.247	2.444	0.148	0.175			
			5.9 <sup>b</sup>										
			5.5 <sup>a1</sup>				2.34 <sup>a1</sup>		0.158 <sup>a1</sup>				
0.25	0.0	$\text{Cd}_{0.25}\text{Zn}_{0.75}\text{Te}$	7.143		7.491		2.612	2.837	0.204	0.219			
			6.873		7.200		2.565	2.683	0.197	0.208			
			6.431		6.877		2.496	2.622	0.187	0.200			
			6.229		6.504		2.413	2.550	0.177	0.190			
			5.747		6.054		2.279	2.456	0.156	0.180			
			5.26 <sup>a3</sup>				2.29 <sup>a3</sup>						
			0.50	0.0	$\text{Cd}_{0.50}\text{Zn}_{0.50}\text{Te}$	7.171		7.619		2.640	2.923	0.212	0.224
						6.888		7.283		2.587	2.720	0.205	0.216
						6.503		6.965		2.530	2.660	0.197	0.210
						6.290		6.550		2.441	2.617	0.188	0.197
5.774		6.132					2.357	2.478	0.164	0.188			
0.75	0.0	$\text{Cd}_{0.75}\text{Zn}_{0.25}\text{Te}$	7.196		7.723		2.665	2.956	0.215	0.231			
			6.967		7.331		2.621	2.770	0.210	0.224			
			6.669		7.007		2.563	2.709	0.206	0.218			
			6.344		6.684		2.481	2.646	0.191	0.204			
			5.798		6.194		2.377	2.504	0.172	0.191			
1.0	0.0	CdTe	7.218		7.799		2.703	2.997	0.219	0.243			
			7.2 <sup>a</sup>										
			6.70 <sup>b1,c1</sup>				2.85 <sup>f1</sup>		0.224 <sup>f1</sup>				
			9.02 <sup>d1</sup>				2.88 <sup>g1</sup>						
			7.3 <sup>e1</sup>				2.46 <sup>a2</sup>						
			8.21 <sup>f1</sup>										
			6.08 <sup>a2</sup>										
			7.004		7.411		2.663	2.822	0.216	0.229			
			6.60 <sup>a2</sup>				2.57 <sup>a2</sup>						
			6.727		7.321		2.606	2.773	0.212	0.223			
5.95 <sup>a2</sup>				2.44 <sup>a2</sup>									
6.482		6.829		2.537	2.715	0.203	0.215						
5.81 <sup>a2</sup>				2.41 <sup>a2</sup>									
1.0	0.0	CdSe	5.823		6.243		2.418	2.593	0.177	0.197			
			5.8 <sup>b</sup>										
			6.26 <sup>b1</sup>				2.56 <sup>f1</sup>		0.195 <sup>f1</sup>				
			5.4 <sup>c1</sup>				2.29 <sup>a2</sup>						
			5.68 <sup>d1</sup>										
			5.8 <sup>e1</sup>										
			6.75 <sup>f1</sup>										
5.25 <sup>a2</sup>													

Experimental data: <sup>a</sup>Ref. [27], <sup>b</sup>Ref. [26]

Earlier theoretical data: <sup>a1</sup>Ref. [97], <sup>b1</sup>Ref. [72], <sup>c1</sup>Ref. [68], <sup>d1</sup>Ref. [59], <sup>e1</sup>Ref. [69], <sup>f1</sup>Ref. [100], <sup>g1</sup>Ref. [67], <sup>a2</sup>Ref. [87], <sup>a3</sup>Ref. [98]

respect to earlier mBJ-based theoretical data [98] due to our higher calculated mBJ-based bandgap compared with the corresponding earlier study.

From Table 6, the following facts can be noted: The  $\varepsilon_1(0)$ ,  $n(0)$ , and  $R(0)$  values calculated for any of the specimens using both XC functionals exhibit the trends  $\varepsilon_1(0)^{\text{EV-GGA}} > \varepsilon_1(0)^{\text{mBJ}}$ ,  $n(0)^{\text{EV-GGA}} > n(0)^{\text{mBJ}}$ , and  $R(0)^{\text{EV-GGA}} > R(0)^{\text{mBJ}}$ , whereas our calculated fundamental bandgaps follow the trend  $E_g^{\text{mBJ}} > E_g^{\text{EV-GGA}}$  in Table 4 in this situation. The aforesaid correlation between  $\varepsilon_1(0)$  and  $E_g$  can be clarified by the approximate relation among them, as proposed by Penn [129]:

$$\varepsilon_1(0) \approx 1 + \left( \frac{\hbar\omega_p}{E_g} \right)^2. \quad (4)$$

Equation 4 indicates an approximate inverse proportionality between  $\varepsilon_1(0)$  and the square of  $E_g$ . Therefore, the  $\varepsilon_1(0)$  of a material increases with a decrease in the bandgap, and vice versa.

For any specimen, the approximate relationship between  $n(0)$  and  $\varepsilon_1(0)$  is [127]

$$n(0) \approx \sqrt{\varepsilon_1(0)}. \quad (5)$$

One can establish all the aforesaid correlations between  $n(0)$  and  $E_g$  using the following relation between them, obtained by combining Eqs. 4 and 5:

$$n(0) \approx \sqrt{1 + \left( \frac{\hbar\omega_p}{E_g} \right)^2}. \quad (6)$$

Equation 6 indicates an approximate inverse proportionality between  $n(0)$  and  $E_g$ . Therefore, an increase in  $E_g$  results in a decrease in  $n(0)$ , and vice versa, in any semiconductor.

The extinction coefficient  $k(\omega)$  becomes zero for each specimen at zero incident frequency, so the relationship between  $n(0)$  and  $R(0)$ , using Eq. SQ10, becomes

$$R(0) = \left[ \frac{1 - n(0)}{1 + n(0)} \right]^2. \quad (7)$$

Finally, the aforesaid correlations between  $E_g$  and  $R(0)$  can also be established using the following relation between them, obtained by combining Eqs. 6 and 7:

$$R(0) = \left[ \frac{1 - \sqrt{1 + \left( \frac{\hbar\omega_p}{E_g} \right)^2}}{1 + \sqrt{1 + \left( \frac{\hbar\omega_p}{E_g} \right)^2}} \right]^2. \quad (8)$$

Clearly, Eq. 8 indicates that an increase in  $E_g$  will result in a reduction in  $R(0)$ , and vice versa, in any semiconductor.

The critical points in the  $\varepsilon_2(\omega)$ ,  $k(\omega)$ ,  $\sigma(\omega)$ , and  $\alpha(\omega)$  spectra are the threshold incident energy  $E_c$  (eV) at which each of these optical parameters starts responding to the incident radiation. Note that a semiconductor specimen with higher fundamental bandgap requires a higher critical point energy in its  $\varepsilon_2(\omega)$  and  $k(\omega)$  spectra, and vice versa, according to the Kramers–Kronig transformations between  $\varepsilon_1(\omega)$  and  $\varepsilon_2(\omega)$  [Eqs. SQ3 and SQ4] as well as between  $n(\omega)$  and  $k(\omega)$  [Eqs. SQ6 and SQ7], respectively. Since  $\sigma(\omega)$  is proportional to  $\varepsilon_2(\omega)$  and  $\alpha(\omega)$  is proportional to  $k(\omega)$  according to Eqs. SQ11 and SQ13, respectively, a similar bandgap dependence of the critical points is observed in the  $\sigma(\omega)$  and  $\alpha(\omega)$  spectra. The critical points in the aforesaid spectra of all the binary, ternary, and quaternary specimens in the  $\text{Cd}_x\text{Zn}_{1-x}\text{Se}_y\text{Te}_{1-y}$  quaternary system calculated using both the mBJ and EV-GGA functionals are presented in Table 7, but no experimental critical point data for any of these specimens are available for comparison. On the other hand, earlier calculated critical points in the  $\varepsilon_2(\omega)$ ,  $k(\omega)$ ,  $\sigma(\omega)$ , and  $\alpha(\omega)$  spectra of only the binary specimens CdSe and CdTe are available in literature [100]. It is observed from Table 7 that each of our mBJ- and EV-GGA-based computed critical points in each of the  $\varepsilon_2(\omega)$ ,  $k(\omega)$ ,  $\sigma(\omega)$ , and  $\alpha(\omega)$  spectra of CdSe and CdTe are much higher than the respective earlier theoretically reported critical points for CdSe and CdTe [100]. This is because our bandgaps for CdSe and CdTe calculated using both XC functionals are much higher than the respective bandgaps reported in that earlier theoretical study [100]. It is clear from Table 7 that our calculated critical point in each of the  $\varepsilon_2(\omega)$ ,  $k(\omega)$ ,  $\sigma(\omega)$ , and  $\alpha(\omega)$  spectra of any specimen obeys the trend  $E_c^{\text{mBJ}} > E_c^{\text{EV-GGA}}$ , since our bandgaps calculated with both XC functionals follow the trend  $E_g^{\text{mBJ}} > E_g^{\text{EV-GGA}}$  in Table 4.

### 3.3.3 The concentration dependence of the zero-frequency limits and critical points

The zero-frequency limits  $\varepsilon_1(0)$ ,  $n(0)$ , and  $R(0)$  as well as the critical points in the  $\varepsilon_2(\omega)$ ,  $k(\omega)$ ,  $\sigma(\omega)$ , and  $\alpha(\omega)$  spectra of the specimens in the  $\text{Cd}_x\text{Zn}_{1-x}\text{Se}_y\text{Te}_{1-y}$  quaternary system are strongly dependent on the cationic (Cd) and anionic (Se) concentrations  $x$  and  $y$ , respectively. The concentration dependence of these optical constants is studied in this subsection.

At each of the five fixed values of the cationic (Cd) concentration  $x$ , each of the zero-frequency limits  $\varepsilon_1(0)$ ,  $n(0)$ , and  $R(0)$  calculated using both XC functionals decreases, while the critical points in each of the  $\varepsilon_2(\omega)$ ,  $k(\omega)$ ,  $\sigma(\omega)$ , and  $\alpha(\omega)$  spectra increase with increasing anionic (Se) concentration  $y$ , as observed from Tables 6 and 7, respectively. On the other hand, at each of the five fixed anionic (Se) concentrations  $y$ , each of the  $\varepsilon_1(0)$ ,  $n(0)$ , and  $R(0)$  calculated

**Table 7** The critical points in the  $\varepsilon_2(\omega)$ ,  $k(\omega)$ ,  $\sigma(\omega)$ , and  $\alpha(\omega)$  spectra of the binary, ternary, and quaternary specimens in the  $\text{Cd}_x\text{Zn}_{1-x}\text{Se}_y\text{Te}_{1-y}$  system calculated using the mBJ and EV-GGA functionals

x	y	Specimen	Critical point (eV) in the spectra of							
			$\varepsilon_2(\omega)$		$k(\omega)$		$\sigma(\omega)$		$\alpha(\omega)$	
			mBJ	EV-GGA	mBJ	EV-GGA	mBJ	EV-GGA	mBJ	EV-GGA
0.0	0.0	ZnTe	2.176	1.554	2.136	1.563	2.244	1.717	2.354	1.772
	0.25	$\text{ZnSe}_{0.25}\text{Te}_{0.75}$	2.231	1.595	2.372	1.610	2.386	1.813	2.594	1.800
	0.50	$\text{ZnSe}_{0.50}\text{Te}_{0.50}$	2.345	1.664	2.581	1.789	2.498	1.895	2.735	1.882
	0.75	$\text{ZnSe}_{0.75}\text{Te}_{0.25}$	2.536	1.727	2.717	1.855	2.674	1.963	2.871	1.961
	1.0	ZnSe	2.852	1.952	2.932	2.032	3.027	2.042	2.962	2.063
0.25	0.0	$\text{Cd}_{0.25}\text{Zn}_{0.75}\text{Te}$	2.063	1.383	1.918	1.310	2.054	1.555	2.136	1.483
	0.25	$\text{Cd}_{0.25}\text{Zn}_{0.75}\text{Se}_{0.25}\text{Te}_{0.75}$	2.197	1.438	2.246	1.392	2.222	1.583	2.258	1.510
	0.50	$\text{Cd}_{0.25}\text{Zn}_{0.75}\text{Se}_{0.50}\text{Te}_{0.50}$	2.326	1.499	2.354	1.446	2.436	1.610	2.363	1.537
	0.75	$\text{Cd}_{0.25}\text{Zn}_{0.75}\text{Se}_{0.75}\text{Te}_{0.25}$	2.489	1.515	2.430	1.483	2.572	1.631	2.542	1.619
	1.0	$\text{Cd}_{0.25}\text{Zn}_{0.75}\text{Se}$	2.695	1.564	2.513	1.537	2.789	1.673	2.664	1.700
0.50	0.0	$\text{Cd}_{0.50}\text{Zn}_{0.50}\text{Te}$	1.710	1.247	1.755	1.202	1.863	1.346	1.945	1.374
	0.25	$\text{Cd}_{0.50}\text{Zn}_{0.50}\text{Se}_{0.25}\text{Te}_{0.75}$	1.981	1.282	1.867	1.229	2.018	1.374	2.046	1.401
	0.50	$\text{Cd}_{0.50}\text{Zn}_{0.50}\text{Se}_{0.50}\text{Te}_{0.50}$	2.228	1.313	2.049	1.260	2.146	1.401	2.173	1.428
	0.75	$\text{Cd}_{0.50}\text{Zn}_{0.50}\text{Se}_{0.75}\text{Te}_{0.25}$	2.364	1.345	2.218	1.292	2.227	1.428	2.254	1.455
	1.0	$\text{Cd}_{0.50}\text{Zn}_{0.50}\text{Se}$	2.544	1.374	2.381	1.346	2.381	1.483	2.381	1.510
0.75	0.0	$\text{Cd}_{0.75}\text{Zn}_{0.25}\text{Te}$	1.574	1.167	1.619	1.156	1.782	1.265	1.837	1.292
	0.25	$\text{Cd}_{0.75}\text{Zn}_{0.25}\text{Se}_{0.25}\text{Te}_{0.75}$	1.737	1.180	1.710	1.174	1.809	1.292	1.937	1.319
	0.50	$\text{Cd}_{0.75}\text{Zn}_{0.25}\text{Se}_{0.50}\text{Te}_{0.50}$	1.992	1.202	1.891	1.199	1.837	1.319	2.064	1.346
	0.75	$\text{Cd}_{0.75}\text{Zn}_{0.25}\text{Se}_{0.75}\text{Te}_{0.25}$	2.201	1.215	1.990	1.203	1.891	1.346	2.191	1.374
	1.0	$\text{Cd}_{0.75}\text{Zn}_{0.25}\text{Se}$	2.425	1.249	2.099	1.233	2.209	1.374	2.303	1.401
1.0	0.0	CdTe	1.465	1.074	1.483	1.036	1.646	1.122	1.674	1.236
			0.82 <sup>a</sup>		0.70 <sup>a</sup>		0.95 <sup>a</sup>		1.04 <sup>a</sup>	
	0.25	$\text{CdSe}_{0.25}\text{Te}_{0.75}$	1.510	1.127	1.537	1.117	1.727	1.238	1.755	1.265
	0.50	$\text{CdSe}_{0.50}\text{Te}_{0.50}$	1.565	1.154	1.692	1.152	1.782	1.265	1.782	1.292
	0.75	$\text{CdSe}_{0.75}\text{Te}_{0.25}$	1.673	1.182	1.846	1.186	1.837	1.292	1.837	1.319
	1.0	CdSe	2.357	1.238	1.958	1.210	2.146	1.333	2.162	1.392
		0.82 <sup>a</sup>		0.70 <sup>a</sup>		0.95 <sup>a</sup>		1.04 <sup>a</sup>		

Earlier theoretical data: <sup>a</sup>Ref. [100]

using both XC functionals increases, while the critical points in each of the  $\varepsilon_2(\omega)$ ,  $k(\omega)$ ,  $\sigma(\omega)$ , and  $\alpha(\omega)$  spectra decrease with increasing cationic (Cd) concentration  $x$ , as presented in Tables 6 and 7, respectively. Note that, in the former type of variation, our bandgap calculated using both the mBJ and EV-GGA functional increases, while the reverse trend is observed in the latter type of bandgap variation. Therefore, both variation trends for each of  $\varepsilon_1(0)$ ,  $n(0)$ , and  $R(0)$  as well as the critical points in each of the said spectra with the cationic ( $x$ ) and anionic ( $y$ ) concentration are strongly related to the concentration ( $x/y$ ) dependence of the bandgap. An increase in the bandgap results in a decrease in each of these zero-frequency limits and an increase in the critical points, respectively, and vice versa. Therefore, this bandgap dependence of each of  $\varepsilon_1(0)$ ,  $n(0)$ , and  $R(0)$  is again well supported by Eqs. 4, 6, and 8, respectively, while that of each of the critical points in the said spectra is supported by the

Kramers–Kronig transformations between  $\varepsilon_1(\omega)$  and  $\varepsilon_2(\omega)$  [Eqs. SQ3 and SQ4], between  $n(\omega)$  and  $k(\omega)$  [Eqs. SQ6 and SQ7], as well as Eqs. SQ11 and SQ13, respectively.

### 3.4 Substrate selection for growth of quaternary alloys

This section investigates the possibility of lattice matching between  $\text{Cd}_x\text{Zn}_{1-x}\text{Se}_y\text{Te}_{1-y}$  and ZnTe, InAs, GaSb, and InP, to test their acceptability as appropriate substrates for the growth of these quaternary alloys. This is due to the fact that the lattice constants of some of these quaternary alloys are very close to these substrates. ZnTe, InAs, GaSb, and InP are also direct-bandgap semiconductors in their zincblende crystallographic phase. Moreover, they are available with a high degree of purity. Therefore, they can be chosen as suitable substrates for the growth of some of the  $\text{Cd}_x\text{Zn}_{1-x}\text{Se}_y\text{Te}_{1-y}$

quaternary alloys. The lattice parameters of ZnTe, InAs, GaSb, and InP are taken to be 6.104 Å, 6.058 Å, 6.095 Å, and 5.868 Å, respectively.

The lattice constant  $a(x, y)$  for each quaternary alloy is determined using the modified Vegard's rule as [130]

$$a(x, y) = xy a_{\text{CdSe}} + (1-x)y a_{\text{ZnSe}} + x(1-y) a_{\text{CdTe}} + (1-x)(1-y) a_{\text{ZnTe}}, \quad (9)$$

where  $a_{\text{CdSe}}$ ,  $a_{\text{CdTe}}$ ,  $a_{\text{ZnSe}}$ , and  $a_{\text{ZnTe}}$  are the lattice constants of CdSe, CdTe, ZnSe, and ZnTe, respectively.

Now, substituting  $a(x, y)$  with the lattice constant of ZnTe in Eq. 9, the condition for lattice matching of  $\text{Cd}_x\text{Zn}_{1-x}\text{Se}_y\text{Te}_{1-y}$  with this diatomic compound is

$$y = \frac{0.079 + 0.435x}{0.445 - 0.025x} \quad (0 \leq x \leq 0.796). \quad (10)$$

Meanwhile, substituting  $a(x, y)$  with the lattice constant of InAs in Eq. 9, the condition for lattice matching of  $\text{Cd}_x\text{Zn}_{1-x}\text{Se}_y\text{Te}_{1-y}$  with InAs is

$$y = \frac{0.051 + 0.369x}{0.421 - 0.061x} \quad (0 \leq x \leq 0.861). \quad (11)$$

Also, substituting  $a(x, y)$  with the lattice constant of GaSb in Eq. 9, the condition for lattice matching of  $\text{Cd}_x\text{Zn}_{1-x}\text{Se}_y\text{Te}_{1-y}$  with this diatomic compound is

$$y = \frac{0.013 + 0.369x}{0.421 - 0.061x} \quad (0 \leq x \leq 0.948). \quad (12)$$

Similarly, the condition for lattice matching of  $\text{Cd}_x\text{Zn}_{1-x}\text{Se}_y\text{Te}_{1-y}$  with InP, obtained by substituting  $a(x, y)$  with the lattice constant of InP in Eq. 9, is

$$y = \frac{0.240 + 0.369x}{0.421 - 0.061x} \quad (0 \leq x \leq 0.420). \quad (13)$$

The results of this study show that five quaternaries achieve less than 5% lattice mismatch to the ZnTe substrate, corresponding to the specific concentrations  $x=0.25$ ,  $y=0.25$ ;  $x=0.50$ ,  $y=0.25$ ;  $x=0.50$ ,  $y=0.50$ ;  $x=0.75$ ,  $y=0.50$ ;  $x=0.75$ ,  $y=0.75$  with lattice mismatch values of 1.85%, 3.72%, 2.03%, 3.70%, and 1.87%, respectively. Again, there are five quaternaries achieving less than 5% lattice mismatch to the InAs substrate, corresponding to the specific concentrations  $x=0.25$ ,  $y=0.25$ ;  $x=0.50$ ,  $y=0.25$ ;  $x=0.50$ ,  $y=0.50$ ;  $x=0.75$ ,  $y=0.50$ ;  $x=0.75$ ,  $y=0.75$  with lattice mismatch values of 1.89%, 3.68%, 2.81%, 4.34%, and 2.64%, respectively.

It is observed that there are six quaternary alloys, corresponding to concentrations  $x=0.25$ ,  $y=0.25$ ;  $x=0.50$ ,  $y=0.25$ ;  $x=0.50$ ,  $y=0.50$ ;  $x=0.75$ ,  $y=0.25$ ;  $x=0.75$ ,  $y=0.50$ ;  $x=0.75$ ,  $y=0.75$ , which achieve less than 5% lattice mismatch to the GaSb substrate, with values of 1.26%, 3.04%, 2.17%, 4.38%, 3.69%, and 2.00%, respectively.

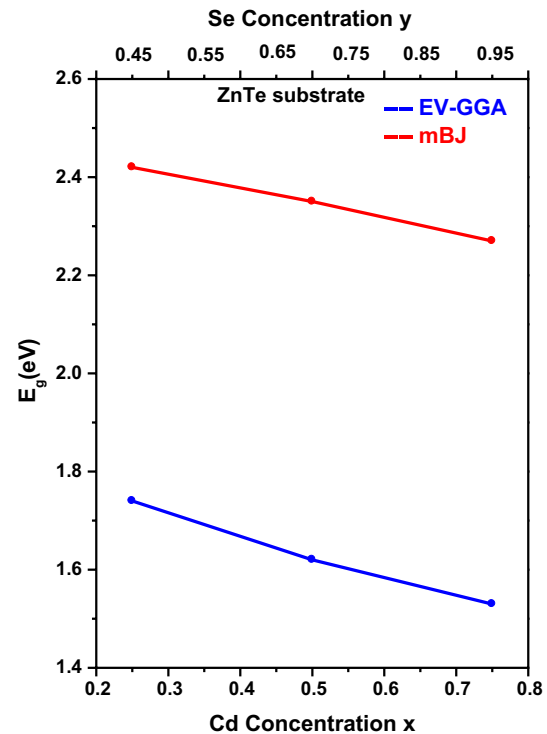


**Fig. 10** The energy bandgap of the  $\text{Cd}_x\text{Zn}_{1-x}\text{Se}_y\text{Te}_{1-y}$  quaternary alloys lattice matched to ZnTe as a function of the Cd concentration  $x$  as calculated using the mBJ (red line) and EV-GGA (blue line) functional (Color figure online)

Finally, in the case of the InP substrate, it is found that there are only two quaternaries that achieve less than 5% lattice mismatch, corresponding to concentrations  $x=0.25$ ,  $y=0.50$ ;  $x=0.25$ ,  $y=0.75$ , with corresponding lattice mismatch values of 4.15% and 2.17%, respectively.

Equation 10 provides a line of  $x$  and  $y$  concentrations along which the corresponding alloys are lattice matched to ZnTe; three different concentrations are considered along the straight line: (0.25, 0.427); (0.50, 0.685); (0.75, 0.951). Equation 11 provides a line of  $x$  and  $y$  concentrations along which the corresponding alloys are lattice matched to InAs; the corresponding three different concentrations considered along the straight line are (0.25, 0.352); (0.50, 0.602); (0.75, 0.873). Again, Eq. 12 provides another line of  $x$  and  $y$  concentrations along which the corresponding alloys are lattice matched to GaSb, and the corresponding three different concentrations considered along the straight line are (0.25, 0.259); (0.50, 0.506); (0.75, 0.772).

Figures 10, 11, and 12 show the energy bandgap as a function of the cadmium ( $x$ ) concentration along the ZnTe, InAs, and GaSb matching line, respectively, as calculated using both the EV-GGA and mBJ functionals. These results reveal that one can tune the cationic ( $x$ ) and anionic ( $y$ ) concentrations in the quaternary alloys to achieve a range of

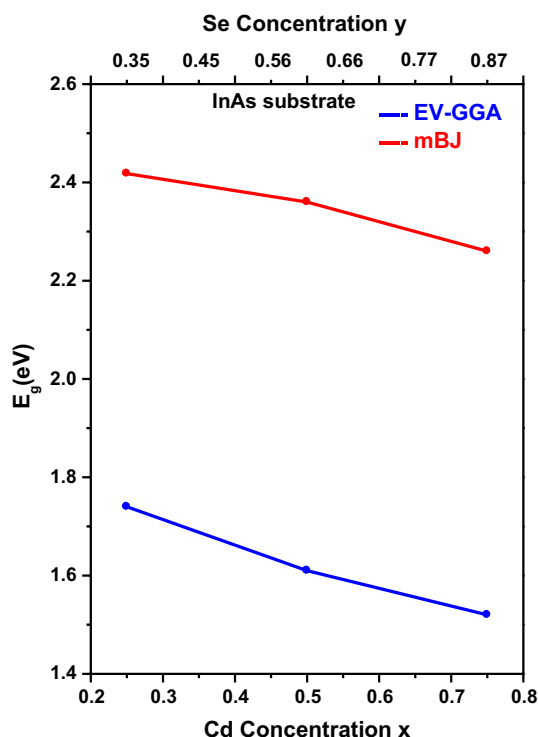


**Fig. 11** The energy bandgap of the  $\text{Cd}_x\text{Zn}_{1-x}\text{Se}_y\text{Te}_{1-y}$  quaternary alloys lattice matched to InAs as a function of the Cd concentration  $x$  as calculated using the mBJ (red line) and EV-GGA (blue line) functional (Color figure online)

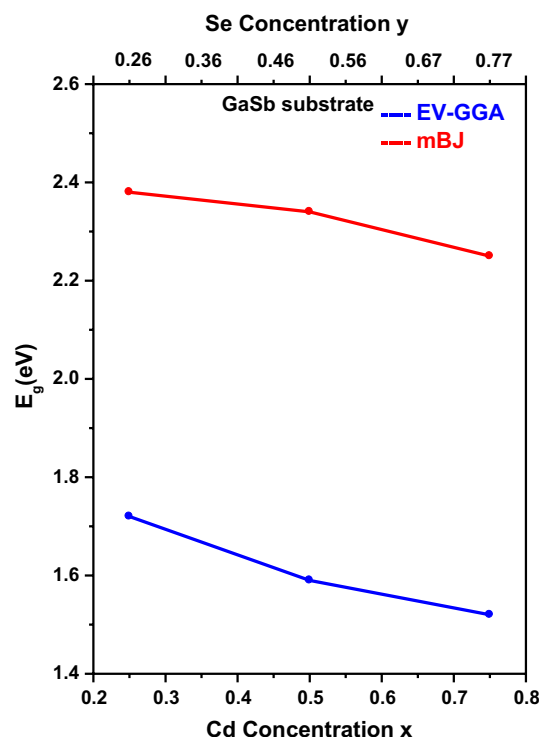


**Fig. 12** The energy bandgap of the  $\text{Cd}_x\text{Zn}_{1-x}\text{Se}_y\text{Te}_{1-y}$  quaternary alloys lattice matched to GaSb as a function of the Cd concentration  $x$  as calculated using the mBJ (red line) and EV-GGA (blue line) functional (Color figure online)

bandgap and hence optical properties for the alloys grown on ZnTe, InAs, and GaSb substrates. It is clear from Fig. 10 that, when using the EV-GGA functional, the bandgap ranges from 1.53 to 1.74 eV, while it ranges from 2.25 to 2.42 eV with the mBJ functional in the case of the ZnTe substrate. From Fig. 11, note that the bandgap ranges from 1.52 to 1.74 eV for the EV-GGA functional, but from 2.26 to 2.40 eV for the mBJ functional in the case of the InAs substrate. Finally, from Fig. 12, it is clear that the bandgap ranges from 1.52 to 1.73 eV for the EV-GGA functional, but from 2.24 to 2.38 eV with the mBJ functional in the case of the GaSb substrate.

## 4 Conclusions

The structural and optoelectronic properties of the specimens in the  $\text{Cd}_x\text{Zn}_{1-x}\text{Se}_y\text{Te}_{1-y}$  quaternary system are calculated as a function of the compositions  $x$  and  $y$  by employing the DFT-based FP-LAPW approach. The XC potentials are calculated using the PBE-GGA functional for the structural properties and both the mBJ and EV-GGA functionals for the optoelectronic properties. Considering the whole range of anionic concentration ( $y$ ) at each of the fixed cationic

concentrations ( $x$ ) and vice versa, the  $\text{Cd}_x\text{Zn}_{1-x}\text{Se}_y\text{Te}_{1-y}$  quaternary system is divided into five binary–ternary and ternary–quaternary subsystems in each category, and the concentration dependence of the said properties is studied in detail. The dependence of the lattice constant, bulk modulus, and bandgap on the concentrations  $x$  and  $y$  exhibits nonlinear behavior. A decrease in the lattice constant and an increase in the bulk modulus are observed with increasing anionic concentration  $y$  at each cationic concentration  $x$ , while the reverse is observed with increasing cationic concentration  $x$  at each fixed anionic concentration  $y$ . A direct bandgap ( $\Gamma$ – $\Gamma$ ) is observed for each of the specimens in the  $\text{Cd}_x\text{Zn}_{1-x}\text{Se}_y\text{Te}_{1-y}$  quaternary system. At each of the cationic concentrations  $x$ , the bandgap increases with increasing anionic concentration  $y$ , while the opposite is observed for the variation of the bandgap with the cationic concentration  $x$  at each of the anionic concentrations  $y$ . The frequency response of different optical parameters is computed. It is observed that the zero-frequency limit in each of the  $\epsilon_1(\omega)$ ,  $n(\omega)$ , and  $R(\omega)$  spectra shows the opposite trend, while the critical point in each of the  $\epsilon_2(\omega)$ ,  $k(\omega)$ ,  $\sigma(\omega)$ , and  $\alpha(\omega)$  spectra shows the same trend, with respect to the variation of the bandgap with the concentrations  $x$  and  $y$ . Finally, the  $\text{Cd}_x\text{Zn}_{1-x}\text{Se}_y\text{Te}_{1-y}$  quaternary alloys that are lattice matched

to the ZnTe, InAs, GaSb, and InP substrates are investigated, revealing that these materials can act as suitable substrates for the growth of some of the said quaternary alloys. These results for the quaternary alloys should be useful for the design of optoelectronic devices for operation in the visible and ultraviolet (UV) spectral ranges, when they are lattice matched to ZnTe, InAs, GaSb, and InP as substrates.

**Acknowledgements** The authors are grateful to UGC, Govt. of India for financial support to carry out this research work through financial assistance under UGC–SAP program 2016 [ref. no. F.530/23/DRS-I/2018 (SAP-I)].

## References

- Nelmes, R.J., McMohan, M.I.: Structural transitions in the group IV, III-V, and II-VI semiconductors under pressure. *Semicond. Semimetals* **54**, 145–246 (1998)
- Eckelt, P.: Energy band structures of cubic ZnS, ZnSe, ZnTe, and CdTe (Korringa-Kohn-Rostoker method). *Phys. Stat. Sol.* **23**, 307–312 (1967)
- Wang, J., Isshiki, M.: Wide-Band-gap II–VI Semiconductors: Growth and properties. In: Kasper, S., Capper, P. (eds.) *Springer Handbook of Electronic and Photonic Materials*, pp. 325–342. Springer, Berlin (2006)
- Adachi, S.: *Properties of Group-IV, III–V and II–VI Semiconductors*. Wiley, London (2005)
- Van de Walle, C.G.: *Wide-Band-Gap Semiconductors*. North Holland, Amsterdam (1993)
- Huynh, W.U., Dittmer, J.J., Alivisatos, A.P.: Hybrid nanorod-polymer solar cells. *Science* **295**, 2425–2427 (2002)
- Salavei, A., Rimmaudo, I., Piccinelli, F., Romeo, A.: Influence of CdTe thickness on structural and electrical properties of CdTe/CdS solar cells. *Thin Solid Films* **535**, 257–260 (2013)
- Crossay, A., Buecheler, S., Kranz, L., Perrenoud, J., Fella, C.M., Romanyuk, Y.E., Tiwari, A.N.: Spray-deposited Al-doped ZnO transparent contacts for CdTe solar cells. *Solar Energy Mater. Sol. Cells* **101**, 283–288 (2012)
- Nakayama, N., Matsumoto, H., Yamaguchi, K., Ikegami, S., Hioki, Y.: Ceramic thin film CdTe solar cell. *Jpn. J. Appl. Phys.* **15**, 2281–2282 (1976)
- Shieh, F., Saunders, A.E., Korgel, B.A.: General shape control of colloidal CdS, CdSe, CdTe quantum rods and quantum rod heterostructures. *J. Phys. Chem. B* **109**, 8538–8542 (2005)
- Peng, Z.A., Peng, X.G.: Formation of high-quality CdTe, CdSe, and CdS nanocrystals using CdO as precursor. *J. Am. Chem. Soc.* **123**, 183–184 (2001)
- Colvin, V.L., Schlamp, M.C., Alivisatos, A.P.: Light emitting diodes made from cadmium selenide nanocrystals and a conducting polymer. *Nature* **370**, 354–357 (1994)
- Greenham, N.C., Peng, X., Alivisatos, A.P.: Charge separation and transport in conjugated polymer/cadmium selenide nanocrystal composites studied by photoluminescence quenching and photoconductivity. *Synth. Met.* **84**, 545–546 (1997)
- Xi, L.F., Chua, K.H., Zhao, Y.Y., Zhang, J., Xiong, Q.H., Lam, Y.M.: Controlled synthesis of CdE (E = S, Se and Te) nanowires. *RSC Adv.* **2**, 5243–5253 (2012)
- Chen, X., Liu, R., Qiao, S., Mao, J., Du, X.: Synthesis of cadmium chalcogenides nanowires via laser-activated gold catalysts in solution. *Mater. Chem. Phys.* **212**, 408–414 (2018)
- Dabbousi, B.O., Bawendi, M.G., Rubner, O.O.: Electroluminescence from CdSe quantumdot/polymer composites. *Appl. Phys. Lett.* **66**, 1316–1318 (1995)
- Thuy, U.T.D., Toan, P.S., Chi, T.T.K., Khang, D.D., Liem, N.Q.: CdTe quantum dots for an application in the life sciences. *Adv. Nat. Sci. Nanosci. Nanotechnol.* **1**, 045009–045014 (2010)
- Liyanage, W.P.R., Wilson, J.S., Kinzel, E.C., Dorant, B.K.: Fabrication of CdTe nanorod arrays over large area through patterned electrodeposition for efficient solar energy conversion. *Sol. Energy Mater. Sol. Cells* **133**, 260–267 (2015)
- Hasse, M.A., Qui, J., De Puydt, J.M., Cheng, H. Blue-green laser diodes. *Appl. Phys. Lett.* **59**, 1272–1274 (1991)
- Wagner, H.P., Wittmann, S., Schmitzer, H., Stanzl, H.: Phase matched second harmonic generation using thin film ZnTe optical waveguides. *J. Appl. Phys.* **77**, 3637–3640 (1995)
- Tamargo, M.C., Brasil, M.J.S.P., Nahory, R.E., Martin, R.J., Weaver, A.L., Gilchrist, H.L.: MBE growth of the (Zn, Cd)(Se, Te) system for wide-bandgap heterostructure lasers. *Semicond. Sci. Technol.* **6**, A8–A13 (1991)
- Medelung, O.: *Landolt Bornstein: Numerical Data and Functional Relationship in Science and Technology*, vol. 17b. Springer, Berlin (1982)
- Abrikosov, N.K., Bankina, V.B., Poretskaya, L.V., Shelimova, L.E., Skudnova, E.V.: *Semiconducting II-VI IV-VI and V-VI Compounds*. Plenum, New York (1969)
- Strehlow, W.H., Cook, E.L.: *Compilation of energy band gaps in elemental and binary compound semiconductors and insulators*. *J. Phys. Chem. Ref. Data* **2**, 163–199 (1973)
- Harrison, W.A.: *Electronic Structure and the Properties of Solids*. Freeman, San-Francisco (1980)
- Manabe, A., Mitsuishi, A., Yoshinaga, H.: Infrared lattice reflection spectra of II-VI compounds. *Jpn. J. Appl. Phys.* **6**, 593–600 (1967)
- Marple, D.T.F.: Refractive index of ZnSe, ZnTe, and CdTe. *J. Appl. Phys.* **35**, 539–542 (1964)
- Lee, B.H.: Pressure dependence of the second-order elastic constants of ZnTe and ZnSe. *J. Appl. Phys.* **41**, 2988–2990 (1970)
- Berlincourt, D., Jaffe, H., Shiozawa, L.R.: Electroelastic properties of the sulfides, selenides, and tellurides of zinc and cadmium. *Phys. Rev.* **29**, 1009–1017 (1963)
- Kim, Y.D., Klein, M.V., Ren, S.F., Chen, Y.C., Lou, H., Samarth, N., Furdyna, J.K.: Optical properties of zinc-blende CdSe and Zn,Cd& Se films grown on GaAs. *Phys. Rev. B* **49**, 7262–7270 (1994)
- Garcia, V.M., Nair, M.T.S., Nair, P.K., Zingaro, R.A.: Preparation of highly photosensitive CdSe thin films by a chemical bath deposition technique. *Semicond. Sci. Technol.* **11**, 427–432 (1996)
- Toma, O., Ion, L., Girtan, M., Antohe, S.: Optical, morphological and electrical studies of thermally vacuum evaporated CdTe thin films for photovoltaic applications. *Sol. Energy* **108**, 51–60 (2014)
- Okamoto, T., Hayashi, R., Ogawa, Y., Hosono, A., Doi, M.: Fabrication of polycrystalline CdTe thin-film solar cells using carbon electrodes with carbon nanotubes. *Jpn. J. Appl. Phys.* **54**, 04DR01–04DR04 (2015)
- Kim, Y.D., Cooper, S.L., Klein, M.V.: Optical characterization of pure ZnSe films grown on GaAs. *Appl. Phys. Lett.* **62**, 2387–2389 (1993)
- Hsu, C.H., Yan, C.Y., Kao, W.H., Yu, Y.T., Tung, H.H.: Properties of ZnTe thin films on silicon substrate. *Ferroelectrics* **491**, 118–126 (2016)
- Camacho, J., Cantarero, A., Hernández-Calderon, I., Gonzalez, L.: Raman spectroscopy and photoluminescence of ZnTe thin films grown on GaAs. *J. Appl. Phys.* **92**, 6014–6018 (2002)

37. Watanabe, K., Litz, M.T., Korn, M., Ossau, W., Waag, A., Landwehr, G., Schussler, U.: Optical properties of ZnTe/Zn<sub>1-x</sub>Mg<sub>x</sub>Se<sub>y</sub>Te<sub>1-y</sub> quantum wells and epilayers grown by molecular beam epitaxy. *J. Appl. Phys.* **81**, 451–455 (1997)
38. Muthukumarasamy, N., Velumani, S., Balasundaraprabhu, R., Jayakumar, S., Kannan, M.D.: Fabrication and characterization of n-CdSe<sub>0.7</sub>Te<sub>0.3</sub>/p-CdSe<sub>0.15</sub>Te<sub>0.85</sub> solar cell. *Vacuum* **84**, 1216–1219 (2010)
39. MacDonald, B.I., Martucci, A., Rubanov, S., Watkins, S.E., Mulvaney, P., Jasieniak, J.J.: Layer-by-layer assembly of sintered CdSe<sub>x</sub>Te<sub>1-x</sub> nanocrystal solar cells. *ACS Nano* **6**, 5995–6004 (2012)
40. Wen, S., Li, M., Yang, J., Mei, X., Wu, B., Liu, X., Heng, J., Qin, D., Hou, L., Xu, W., Wang, D.: Rationally controlled synthesis of CdSe<sub>x</sub>Te<sub>1-x</sub> alloy nanocrystals and their application in efficient graded bandgap solar cells. *Nanomaterials* **7**, 380–392 (2017)
41. Wen, S., Li, M., Yang, J., Mei, X., Wu, B., Liu, X., Heng, J., Qin, D., Hou, L., Xu, W., Wang, D.: Rationally controlled synthesis of CdSe<sub>x</sub>Te<sub>1-x</sub> alloy nanocrystals and their application in efficient graded bandgap solar cells. *Nanomaterials* (2017). <https://doi.org/10.3390/nano7110380>
42. Asano, H., Arai, K., Kita, M., Omata, T.: Synthesis of colloidal Zn(Te, Se) alloy quantum dots. *Mater. Res. Exp.* **4**, 106501–106510 (2017)
43. Xu, F., Xue, B., Wang, F., Dong, A.: Ternary alloyed ZnSe<sub>x</sub>Te<sub>1-x</sub> nanowires: solution-phase synthesis and band gap bowing. *Chem. Mater.* **27**, 1140–1146 (2015)
44. Lu, J., Liu, H., Zhang, X., Sow, C.H.: One-dimensional nanostructures of II-VI ternary alloys: synthesis, optical properties, and applications. *Nanoscale* (2018). <https://doi.org/10.1039/C8NR05019H>
45. Benkert, A., Schumacher, C., Brunner, K., Neder, R.B.: Monitoring of ZnCdSe layer properties by in situ x-ray diffraction during heteroepitaxy on (001) GaAs substrates. *Appl. Phys. Lett.* **90**, 162105–162107 (2007)
46. Lin, W., Tamargo, M.C., Wei, H.Y., Sarney, W., Salamanca-Riba, L., Fitzpatrick, B.J.: Molecular-beam epitaxy growth and nitrogen doping of hexagonal ZnSe and ZnCdSe/ZnSe quantum well structures on hexagonal ZnMgSSe bulk substrates. *J. Vac. Sci. Tech. B* **18**, 1711–1715 (2000)
47. Kawakami, Y., Yamaguchi, S., Wu, Y.H., Ichino, K., Fujita, S.Z., Fujita, S.G.: Optically pumped blue-green laser operation above room-temperature in Zn<sub>0.80</sub>Cd<sub>0.20</sub>Se-ZnS<sub>0.08</sub>Se<sub>0.92</sub> multiple quantum well structures grown by metalorganic molecular beam epitaxy. *Jpn. J. Appl. Phys.* **30**, L605–L607 (1991)
48. Yilmaz, E.: An investigation of CdZnTe thin films for photovoltaics. *Energy Sources* **34**, 332–335 (2012)
49. Rajesh, G., Muthukumarasamy, N., Velauthapillai, D., Mohanta, K., Ragavendran, V., Batabyal, S.K.: Photoinduced electrical bistability of sputter deposited CdZnTe thin films. *Mater. Res. Exp.* **5**, 026412–026419 (2018)
50. Znamenshchykov, Y.V., Kosyakov, V.V., Opanasyuk, A.S., Kolesnyk, M.M., Fochuk, P.M., Cerskus, A.: Structural and optical properties of Cd<sub>1-x</sub>Zn<sub>x</sub>Te thick films with high Zn concentrations. In: *IEEE 7th International Conference on Nanomaterials: Applications and Properties* (2017)
51. Wang, L., Chen, C., Jin, G., Feng, T., Du, X., Liu, F., Sun, H., Yang, B., Sun, H.: Manipulating depletion region of aqueous-processed nanocrystals solar cells with widened Fermi level offset. *Nano Micro Small* (2018). <https://doi.org/10.1002/sml.201803072>
52. Levy, M., Chowdhury, P.P., Eller, K.A., Chatterjee, A., Nagpal, P.: Tuning ternary Zn<sub>1-x</sub>Cd<sub>x</sub>Te quantum dot composition: engineering electronic states for light-activated superoxide generation as a therapeutic against multidrug-resistant bacteria. *ACS Biomater. Sci. Eng.* **5**, 3111–3118 (2019)
53. Chen, Y.P., Brill, G., Campo, E.M., Hierl, T., Hwang, J.C.M., Dhar, N.K.: Molecular beam epitaxial growth of Cd<sub>1-y</sub>Zn<sub>y</sub>Se<sub>x</sub>Te<sub>1-x</sub> on Si(211). *J. Electron. Mater.* **33**, 498–502 (2004)
54. Nomura, I., Ochiai, Y., Toyomura, N., Manoshiro, A., Kikuchi, A., Kishino, K.: Yellow–green lasing operations of ZnCdTe/MgZnSeTe laser diodes on ZnTe substrates. *Phys. Stat. Sol. B* **241**, 483–486 (2004)
55. Brasil, M.J.S.P., Tamargo, M.C., Nahoty, R.E., Gilchrist, H.L., Martin, R.J.: Zn<sub>1-y</sub>Cd<sub>y</sub>Se<sub>1-x</sub>Tex quaternary wide band-gap alloys: molecular beam epitaxial growth and optical properties. *Appl. Phys. Lett.* **59**, 1206–1208 (1991)
56. Gaikwad, S.A., Tembhurkar, Y.D., Dudhe, C.M.: Study of optical, morphological and electrical properties of CdZnSeTe thin films prepared by spray pyrolysis method. *Int. J. Pure Appl. Phys.* **13**, 339–347 (2017)
57. Roy, U.N., Camarda, G.S., Cui, Y., Gul, R., Yang, G., Zazvorka, J., Dedic, V., Franc, J., James, R.B.: Evaluation of CdZnTeSe as a high quality gamma-ray spectroscopic material with better compositional homogeneity and reduced defects. *Scientific Reports* (2019). <https://doi.org/10.1038/s41598-019-43778-3>
58. Huang, M.Z., Ching, W.Y.: A minimal basis semi-*ab initio* approach to the band structures of semiconductors. *J. Phys. Chem. Solids* **46**, 977–995 (1985)
59. Huang, M.Z., Ching, W.Y.: Calculation of optical excitations in cubic semiconductors. I. Electronic structure and linear response. *Phys. Rev. B* **47**, 9449–9463 (1993)
60. Deligoz, E., Colakoglu, K., Ciftci, Y.: Elastic, electronic, and lattice dynamical properties of CdS, CdSe, and CdTe. *Physica B* **373**, 124–130 (2006)
61. Ouendadji, S., Ghemid, S., Meradji, H., El Haj Hassan, F.: Theoretical study of structural, electronic, and thermal properties of CdS, CdSe and CdTe compounds. *Comput. Mater. Sci.* **50**, 1460–1466 (2011)
62. Sharma, S., Verma, A.S., Sarkar, B.K., Bhandari, R., Jindal, V.K.: First principles study on the elastic and electronic properties of CdX (Se and Te). *AIP Conf. Proc.* **1393**, 229–230 (2011)
63. Wei, S.H., Zhang, S.B.: Structure stability and carrier localization in CdX (X = S, Se, Te) semiconductors. *Phys. Rev. B* **62**, 6944–6947 (2000)
64. Guo, L., Zhang, S., Feng, W., Hu, G., Li, W.: A first-principles study on the structural, elastic, electronic, optical, lattice dynamical, and thermodynamic properties of zinc-blende CdX (X = S, Se, and Te). *J. Alloys Compd.* **579**, 583–593 (2013)
65. Sarkar, S., Pal, S., Sarkar, P., Rosa, A.L., Frauenheim, Th: Self-consistent-charge density-functional tight-binding parameters for Cd–X (X = S, Se, Te) compounds and their interaction with H, O, C, and N. *J. Chem. Theor. Comput.* **7**, 2262–2276 (2011)
66. Cote, M., Zakharov, O., Rubio, A., Cohen, M.L.: *Ab initio* calculations of the pressure-induced structural phase transitions for four II-VI compounds. *Phys. Rev. B* **55**, 13025–13031 (1997)
67. Hosseini, S.M.: Optical properties of cadmium telluride in zinc-blende and wurzite structure. *Phys. B* **403**, 1907–1915 (2008)
68. Corsa, A.D., Baroni, S., Resta, R., Gironcoli, S.: *Ab initio* calculation of phonon dispersions in II-VI semiconductors. *Phys. Rev. B* **47**, 3588–3592 (1993)
69. Zakharov, O., Rubio, A., Blase, X., Cohen, M.L., Loui, S.G.: Quasiparticle band structures of six II-VI compounds: ZnS, ZnSe, ZnTe, CdS, CdSe, and CdTe. *Phys. Rev. B* **50**, 10780–10787 (1994)
70. Chen, X.J., Mintz, A., Hu, J.S., Hua, X.L., Zinck, J., Goddard-III, W.A.: First principles studies of band offsets at heterojunctions and of surface reconstruction using Gaussian dual-space density functional theory. *J. Vac. Sci. Technol. B* **13**, 1715–1727 (1995)
71. Heyd, J., Peralta, J.E., Scuseria, G.E.: Energy band gaps and lattice parameters evaluated with the Heyd-Scuseria-Ernzerhof

- screened hybrid functional. *J. Chem. Phys.* **123**, 174101–174107 (2005)
72. Kootstra, F., de Boeij, P.L., Snijders, J.G.: Application of time-dependent density-functional theory to the dielectric function of various nonmetallic crystals. *Phys. Rev. B* **62**, 7071–7083 (2000)
  73. Wang, C.S., Klein, B.M.: First-principles electronic structure of Si, Ge, GaP, GaAs, ZnS, and ZnSe. I. Self-consistent energy bands, charge densities, and effective masses. *Phys. Rev. B* **24**, 3393–3416 (1981)
  74. Jansen, R.W., Sankey, O.F.: Ab initio linear combination of pseudo-atomic-orbital scheme for the electronic properties of semiconductors: results for ten materials. *Phys. Rev. B* **36**, 6520–6531 (1987)
  75. Fleszar, A., Hanke, W.: Electronic structure of II<sup>B</sup>-VI semiconductors in the *GW* approximation. *Phys. Rev. B* **71**, 045207–045211 (2005)
  76. Oshikiri, M., Aryasetiawan, F.: Band gaps and quasiparticle energy calculations on ZnO, ZnS, and ZnSe in the zinc-blende structure by the *GW* approximation. *Phys. Rev. B* **60**, 10754–10757 (1999)
  77. Lee, G.D., Lee, M.H., Ihm, J.: Role of d electrons in the zinc-blende semiconductors ZnS, ZnSe, and ZnTe. *Phys. Rev. B* **52**, 1459–1462 (1995)
  78. Lee, S.G., Chang, K.J.: First-principles study of the structural properties of MgS-, MgSe-, ZnS-, and ZnSe-based superlattices. *Phys. Rev. B* **52**, 1918–1925 (1995)
  79. Casali, R.A., Christensen, N.E.: Elastic constants and deformation potentials of ZnS and ZnSe under pressure. *Solid State Commun.* **108**, 793–798 (1998)
  80. Gangadharan, R., Jayalakshmi, V., Kalaiselvi, J., Mohan, S., Murugan, R., Palanivel, B.: Electronic and structural properties of zinc chalcogenides ZnX (X = S, Se, Te). *J. Alloys Compd.* **359**, 22–26 (2003)
  81. Smelyansky, V.I., Tse, J.S.: Theoretical study on the high-pressure phase transformation in ZnSe. *Phys. Rev. B* **52**, 4658–4661 (1995)
  82. Okoye, C.M.I.: First-principles study of the electronic and optical properties of zincblende zinc selenide. *Phys. B* **337**, 1–9 (2003)
  83. Khenata, R., Bouhemadou, A., Sahnoun, M., Reshak, A.H., Baltache, H., Rabah, M.: Elastic, electronic and optical properties of ZnS, ZnSe and ZnTe under pressure. *Comput. Mater. Sci.* **38**, 29–38 (2006)
  84. Bilal, M., Shafiq, M., Ahmad, I., Khan, I.: First principle studies of structural, elastic, electronic and optical properties of Zn-chalcogenides under pressure. *J. Semicond.* **35**, 072001–072009 (2014)
  85. Shakil, M., Zafar, M., Ahmed, S., Raza-ur-rehman, Hashmi M., Choudhary, M.A., Iqbal, T.: Theoretical calculations of structural, electronic, and elastic properties of CdSe<sub>1-x</sub>Te<sub>x</sub>: a first principles study. *Chin. Phys. B* **25**, 076104–076110 (2016)
  86. Reshak, A.H., Kityk, I.V., Khenata, R., Auluck, S.: Effect of increasing tellurium content on the electronic and optical properties of cadmium selenide telluride alloys CdSe<sub>1-x</sub>Te<sub>x</sub>: an ab initio study. *J. Alloys Compd.* **509**, 6737–6750 (2011)
  87. Ouendadj, S., Ghemid, S., Bouarissa, N., Meradji, H., El Haj Hassan, F.: Ab initio study of structural, electronic, phase diagram, and optical properties of CdSe<sub>x</sub>Te<sub>1-x</sub> semiconducting alloys. *J. Mater. Sci.* **46**, 3855–3861 (2011)
  88. Bernard, J.E., Zunger, A.: Optical bowing in zinc chalcogenide semiconductor alloys. *Phys. Rev. B* **34**, 5992–5996 (1986)
  89. Ozaki, S., Adachi, S.: Optical constants of ZnSe<sub>x</sub>Te<sub>1-x</sub> ternary alloys. *Jpn. J. Appl. Phys.* **32**, 2620–2625 (1993)
  90. Zaoui, A., Certier, M., Ferhat, M., Pages, O., Aourag, H.: Disorder effects on electronic and optical properties in ZnSe<sub>x</sub>Te<sub>1-x</sub>. *J. Cryst. Growth* **184–185**, 1090–1094 (1998)
  91. El Haj Hassan, F., Amrani, B., Bahsoun, F.: Ab initio investigations of zinc chalcogenides semiconductor alloys. *Phys. B* **391**, 363–370 (2007)
  92. Zhu, Y., Zhang, S.H., Zhang, X.Y., Hao, A.M., Zhang, S.L., Yang, F., Yang, J.K., Liu, R.P.: Structural, elastic, and thermodynamic properties of ZnSe<sub>x</sub>Te<sub>1-x</sub>: a first-principles study. *Comput. Mater. Sci.* **50**, 2745–2749 (2011)
  93. Korozlu, N., Colakoglu, K., Deligoz, E., Ciftci, Y.O.: The structural, electronic and optical properties of Cd<sub>x</sub>Zn<sub>1-x</sub>Se ternary alloys. *Opt. Commun.* **284**, 1863–1867 (2011)
  94. Ameri, M., Fodil, M., Benkabou, F.Z.A., Mahdjoub, Z., Boufadi, F., Bentouaf, A.: Physical properties of the Zn<sub>x</sub>Cd<sub>1-x</sub>Se alloys: ab-initio method. *Mater. Sci. Appl.* **3**, 768–778 (2012)
  95. Mnasri, S., Abdi-Ben Nasrallah, S., Sfina, N., Bouarissa, N., Said, M.: Electronic, lattice vibration and mechanical properties of CdTe, ZnTe, MnTe, MgTe, HgTe and their ternary alloys. *Semicond. Sci. Technol.* **24**, 095008–095015 (2009)
  96. Korozlu, N., Colakoglu, K., Deligoz, E.: Structural, electronic, elastic and optical properties of Cd<sub>x</sub>Zn<sub>1-x</sub>Te mixed crystals. *J. Phys. Condens. Matter* **21**, 175406–175412 (2009)
  97. Bouarissa, N., Atik, Y.: Elastic constants and acoustic wave velocities in Cd<sub>1-x</sub>Zn<sub>x</sub>Te mixed crystals. *Mod. Phys. Lett. B* **22**, 1221–1229 (2008)
  98. Yassin, O.A.: Electronic and optical properties of Zn<sub>0.75</sub>Cd<sub>0.25</sub>S<sub>1-z</sub>Se<sub>z</sub> first-principles calculations based on the Tran-Blaha modified Becke-Johnson potential. *Optik* **127**, 1817–1821 (2016)
  99. Murtaza, G., Ullah, N., Rauf, A., Khenata, R., Bin Omran, S., Sajjad, M., Waheed, A.: First principles study of structural, optical, and electronic properties of zinc mercury chalcogenides. *Mater. Sci. Semicond. Proc.* **30**, 462–468 (2015)
  100. Noor, N.A., Tahir, W., Aslam, F., Shaikat, A.: Ab initio study of structural, electronic and optical properties of Be-doped CdS, CdSe and CdTe compounds. *Physica B* **407**, 943–952 (2012)
  101. Zhou, J.: Recent progress on 2D group II-VI binary chalcogenides ZnX and CdX (X = S, Se, Te): from a theoretical perspective. *Adv. Theory Simul.* (2019). <https://doi.org/10.1002/adts.201900061>
  102. Mezrag, F., Bouarissa, N., Boucenna, M., Hannachi, L.: The effect of zinc concentration upon optical and dielectric properties of Cd<sub>1-x</sub>Zn<sub>x</sub>Se. *Phys. Scr.* **82**, 035702–035706 (2010)
  103. Benkabou, K., Amrane, N., Maachou, M.: Electronic band structure of quaternary alloy Zn<sub>y</sub>Cd<sub>1-y</sub>Se<sub>x</sub>Te<sub>1-x</sub>. *J. Alloys Compd.* **465**, 305–309 (2008)
  104. Hohenberg, P., Kohn, W.: Inhomogeneous electron gas. *Phys. Rev. B* **136**, 864–871 (1964)
  105. Kohn, W., Sham, L.J.: Self-consistent equations including exchange and correlation effects. *Phys. Rev.* **140**, A1133–A1138 (1965)
  106. Reshak, A. H.: Spin-polarized second harmonic generation from the antiferromagnetic CaCoSO single crystal. *Scientific Reports* (2017). <https://doi.org/10.1038/srep46415>
  107. Reshak, A.H.: Ab initio study of TaON, an active photocatalyst under visible light irradiation. *Phys. Chem. Chem. Phys.* **16**, 10558–10565 (2014)
  108. Davydyuk, G.E., Khyzhun, O.Y., Reshak, A.H., Kamarudind, H., Myronchuk, G.L., Danylchuk, S.P., Fedorchuk, A.O., Piskach, L.V., Mozolyuk, M.Yu., Parasyuk, O.V.: Photoelectrical properties and the electronic structure of Tl<sub>1-x</sub>In<sub>1-x</sub>Sn<sub>x</sub>Se<sub>2</sub> (x = 0, 0.1, 0.2, 0.25) single crystalline alloys. *Phys. Chem. Chem. Phys.* **15**, 6965–6972 (2013)
  109. Reshak, A.H., Kogut, Y.M., Fedorchuk, A.O., Zamuruyeva, O.V., Myronchuk, G.L., Parasyuk, O.V., Kamarudin, H., Auluck, S., Plucinski, K.J., Bila, J.: Linear, non-linear optical susceptibilities and the hyperpolarizability of the mixed crystals



- $\text{Ag}_{0.5}\text{Pb}_{1.75}\text{Ge}(\text{S}_{1-x}\text{Se}_x)_4$ : experiment and theory. *Phys. Chem. Chem. Phys.* **15**, 18979–18986 (2013)
110. Reshak, A.H., Stys, D., Auluck, S., Kityk, I.V.: Dispersion of linear and nonlinear optical susceptibilities and the hyperpolarizability of 3-methyl-4-phenyl-5-(2-pyridyl)-1,2,4-triazole. *Phys. Chem. Chem. Phys.* **13**, 2945–2952 (2011)
  111. Reshak, A.H.:  $\text{Fe}_2\text{MnSi}_x\text{Ge}_{1-x}$ : influence thermoelectric properties of varying the germanium content. *RSC Adv.* **4**, 39565–39571 (2014)
  112. Reshak, A.H.: Thermoelectric properties for AA- and AB-stacking of a carbon nitride polymorph ( $\text{C}_3\text{N}_4$ ). *RSC Adv.* **4**, 63137–63142 (2014)
  113. Andersen, O.K.: Linear methods in band theory. *Phys. Rev. B* **42**, 3063–3083 (1975)
  114. Blaha, P., Schwarz, K., Sorantin, P., Trickey, S.K.: Electronic structure calculations of solids using the WIEN2k package for material sciences. *Comput. Phys. Commun.* **59**, 339–415 (1990)
  115. Blaha, P., Schwarz, K., Madsen, G.H., Kvasnicka, D., Luitz, J.: FP-LAPW+lo program for calculating crystal properties, Technische WIEN2K, Austria. (2001)
  116. Perdew, J.P., Burke, K., Ernzerhof, M.: Generalized gradient approximation made simple. *Phys. Rev. Lett.* **77**, 3865–3868 (1996)
  117. Becke, A.D., Johnson, E.R.: A simple effective potential for exchange. *J. Chem. Phys.* **124**, 221101–221104 (2006)
  118. Tran, F., Blaha, P.: Accurate band gaps of semiconductors and insulators with a semilocal exchange-correlation potential. *Phys. Rev. Lett.* **102**, 226401–226404 (2009)
  119. Engel, E., Vosko, S.H.: Exact exchange-only potentials and the virial relation as microscopic criteria for generalized gradient approximations. *Phys. Rev. B* **47**, 13164–13174 (1993)
  120. Kokalj, A.: Computer graphics and graphical user interfaces as tools in simulations of matter at the atomic scale. *Comput. Mater. Sci.* **28**, 155–168 (2003). Code available from <http://www.xcrysden.org/>
  121. Hacini, K., Meradji, H., Ghemid, S., El Haj Hassan, F.: Theoretical prediction of structural, electronic and optical properties of quaternary alloy  $\text{Zn}_{1-x}\text{Be}_x\text{S}_y\text{Se}_{1-y}$ . *Chin. Phys. B* **21**, 036102–036108 (2012)
  122. Murnaghan, F.D.: The compressibility of media under extreme pressures. *Proc. Natl. Acad. Sci. U.S.A.* **30**, 244–247 (1944)
  123. Vegard, L.: The constitution of the mixed crystals and the space filling of the atoms. *Z. Phys.* **5**, 17–26 (1921)
  124. Jobst, B., Hommel, D., Lunz, U., Gerhard, T., Landwehr, G.:  $E_0$  band-gap energy and lattice constant of ternary  $\text{Zn}_{1-x}\text{Mg}_x\text{Se}$  as functions of composition. *Appl. Phys. Lett.* **69**, 97–99 (1996)
  125. Dismukes, J.P., Ekstrom, L., Paff, R.J.: Lattice parameter and density in germanium-silicon alloys. *J. Phys. Chem.* **68**, 3021–3027 (1964)
  126. Fox, M.: *Optical Properties of Solids*. Oxford University Press, Oxford (2001)
  127. Sifi, C., Meradji, H., Silmani, M., Labidi, S., Ghemid, S., Hanneche, E.B., El Haj Hassan, F.: First principle calculations of structural, electronic, thermodynamic and optical properties of  $\text{Pb}_{1-x}\text{Ca}_x\text{S}$ ,  $\text{Pb}_{1-x}\text{Ca}_x\text{Se}$  and  $\text{Pb}_{1-x}\text{Ca}_x\text{Te}$  ternary alloys. *J. Phys. Cond. Matter* **21**, 195401–195409 (2009)
  128. Dadsetani, M., Pourghazi, A.: Optical properties of strontium monochalcogenides from first principles. *Phys. Rev. B* **73**, 195102–195108 (2006)
  129. Penn, D.R.: Wave-number-dependent dielectric function of semiconductors. *Phys. Rev.* **128**, 2093–2097 (1962)
  130. Okuyama, H., Kishita, Y., Ishibashi, A.: Quaternary alloy  $\text{Zn}_{1-x}\text{Mg}_x\text{S}_y\text{Se}_{1-y}$ . *Phys. Rev. B* **57**, 2257–2263 (1998)

**Publisher's Note** Springer Nature remains neutral with regard to jurisdictional claims in published maps and institutional affiliations.